Kobe University Repository : Kernel

タイトル Title	Age control of the first appearance datum for Javanese Homo erectus in the Sangiran area
著者 Author(s)	Matsu'ura, Shuji / Kondo, Megumi / Danhara, Tohru / Sakata, Shuhei / Iwano, Hideki / Hirata, Takafumi / Kurniawan, Iwan / Setiyabudi, Erick / Takeshita, Yoshihiro / Hyodo, Masayuki / Kitaba, Ikuko / Sudo, Masafumi / Danhara, Yugo / Aziz, Fachroel
掲載誌・巻号・ページ Citation	Science,367(6474):210-214
刊行日 Issue date	2020-01-10
資源タイプ Resource Type	Journal Article / 学術雑誌論文
版区分 Resource Version	author
権利 Rights	
DOI	10.1126/science.aau8556
JaLCDOI	
URL	http://www.lib.kobe-u.ac.jp/handle_kernel/90006738

PDF issue: 2021-11-16

Title: Age control of the first appearance datum for Javanese *Homo erectus* in the Sangiran area

Short title: Age of the earliest hominins in Sangiran

One Sentence Summary:

Maximum age of the Sangiran hominins in Indonesia is resolved to ca. 1.3 million years ago, younger than widely accepted.

Authors:

Shuji Matsu'ura[1*], Megumi Kondo[2], Tohru Danhara[3], Shuhei Sakata[4], Hideki Iwano[3], Takafumi Hirata[5], Iwan Kurniawan[6], Erick Setiyabudi[6], Yoshihiro Takeshita[7], Masayuki Hyodo[8,9*], Ikuko Kitaba[10,8], Masafumi Sudo[11], Yugo Danhara[3], Fachroel Aziz[6]

Affiliations:

[1]Department of Anthropology, National Museum of Nature and Science, Tsukuba City, Ibaraki 305-0005, Japan. [2]Laboratory of Physical Anthropology, Ochanomizu University, Bunkyo-ku, Tokyo 112-8610, Japan. [3]Kyoto Fission-Track Corporation, Ltd., Omiya, Kita-ku, Kyoto 603-8832, Japan. [4]Earthquake Research Institude, The University of Tokyo, Bunkyo-ku, Tokyo 113-0032, Japan. [5]Geochemical Research Center, The University of Tokyo, Bunkyo-ku, Tokyo 113-0033, Japan. [6]Centre for Geological Survey, Bandung 40122, Indonesia. [7]Institute of Education, Shinshu University, Nagano City, Nagano 380-8544, Japan. [8]Research Center for Inland Seas, Kobe University, Nada-ku, Kobe 657-8501, Japan. [9]Department of Planetology, Faculty of Science, Kobe University, Nada-ku, Kobe 657-8501, Japan. [10]Research Centre for Palaeoclimatology, Ritsumeikan University, Kusatsu City, Shiga 525-8577, Japan. [11]Institute of Earth and Environmental Science, University of Potsdam, 14476 Golm, Germany.

***Corresponding author. Email: matsu-ur@js2.so-net.ne.jp (S.M); mhyodo@kobe-u.ac.jp (M.H.)**

Abstract:

The chronology of the World Heritage Site of Sangiran in Indonesia is crucial for the understanding of human dispersals and settlement in Asia in the Early Pleistocene (before 780,000 years ago). It has been, however, been controversial, especially for the timing of the earliest hominin migration into the Sangiran region. We used a method of combining fission-track and U–Pb dating, and present here key ages to calibrate the lower (older) Sangiran hominin-bearing horizons. The first appearance datum for the Sangiran hominins is now resolved to be best considered ca. 1.3 million years ago and less than 1.5 million years ago, which is significantly later than the dates widely accepted over the last two decades.

Main Text:

The first appearance datum of *Homo erectus* in the Far East, a hominin species which originated in equatorial Africa or perhaps the Caucasus region of Eurasia (*1–3*), is important in modelling early human dispersals across Asia after the first "Out of Africa" migration. Since the mid-1990s, eastern Asia's oldest hominin remains have been considered to date back to 1.7–1.8 million years ago (Ma) (*4–7*), about half a million years earlier than previously thought (*8–11*). Despite uncertainties (*12*), this chronology and its consequences have been widely recognized as one of paleoanthropology's basic paradigms, that *H. erectus* expanded rapidly to eastern Asia (*1, 13*) after its first appearance at about 1.85 Ma. Furthermore, combined with chronological revisions of *H. erectus* sites in China, different dispersal dynamics were suggested for southeastern and northeastern Asia (*14, 15*): an earlier (> 1.5 Ma) *H. erectus* dispersal along a southern route to equatorial southeast Asia, and a later (< ca. 1.3 Ma) dispersing population along a northerly route to northeast Asia. Although the hypothesis of a later dispersal to northeastern Asia disagrees with current Chinese hominin fossil chronologies (*6, 7*), an early dispersal into southeast Asia has been based on evidence from the Sangiran area (Indonesia) where, on the basis of $^{40}Ar/^{39}Ar$ geochronology, *H. erectus* has been contended to date to ca. 1.6 Ma (*5*). However, other $^{40}Ar/^{39}Ar$ ages (*16, 17*) and a newly refined magnetic polarity stratigraphy of the Sangiran area (*18*) failed to support this chronology. This calls for reevaluation of the 1.6 Ma Sangiran *H. erectus* age. Here we report U–Pb and fission-track dates of volcaniclastic layers in and just above the Grenzbank zone, a key bed of the lower Sangiran hominin-bearing horizons. We also present dates of a marker tuff lying below the hominin-bearing horizons. Our results provide reliable age control points to infer the first appearance datum for Javanese *Homo erectus* in Sangiran.

Sangiran in Central Java (Fig. 1A) is one of the most productive sites in paleoanthropology. It has produced a steady stream of *H. erectus* finds since 1936, now totaling over 100 hominin specimens. However, it lacks an accepted chronostratigraphy. Geologically, the Sangiran area is a dome-like structure, extending 8 km north-south and 4 km east-west (Fig. 1B). The dome is truncated by erosion, exposing a concentric pattern of strata, with older strata surrounded by younger strata (*19*) (Fig. 1B). The exposed sediments, over 300 m thick, are divided into four units (*19*). The marine Puren Formation lies at the base (Fig. 1C). The overlying Sangiran Formation consists of the Lower Lahar (volcanic breccia) at its lowermost part and the "black clay." The latter comprises shallow marine to lagoonal sediments and overlying lacustrine sediments that are partly pedogenized. The Sangiran Formation is overlain by the Bapang Formation, the base of which is known as the Grenzbank zone, a fossiliferous unit of carbonate-cemented gravelly sands. The Bapang Formation is further overlain by the Pohjajar Formation (Fig. 1C). The upper two formations are primarily fluviatile sediments intercalating many layers of pumice, volcanic ash, and lahar.

Previous lithostratigraphic and geochemical investigations have revealed that the hominin-bearing horizons of the Sangiran area could range from the Upper Tuff of the Bapang Formation down to Tuff 11 of the uppermost Sangiran Formation (*19*) or plausibly to the lower levels in the Upper Sangiran Formation (*8, 20*) (Fig. 1C). A systematic investigation of the chronostratigraphy of this sequence was first conducted in the late 1970s to early 1990s, including fission-track dating and magnetostratigraphic analysis, suggesting a hominin time span of ca. 0.8 Ma to 1.1 Ma (*10, 19*) or possibly to ca. 1.3 Ma (*8*). However, in 1994, a substantially

older $^{40}Ar/^{39}Ar$ date of 1.66 Ma was reported for pumices presumably overlying two allegedly oldest hominin remains (*4*). Although this date has been questioned because of the uncertain stratigraphic relationship between the dated pumice and the hominin specimens (*5*, *21*, *22*), Larick *et al.* (*5*) subsequently reported a series of hornblende $^{40}Ar/^{39}Ar$ dates that supported the older chronology and placed the Sangiran hominin-bearing sequence from >1.5 Ma to about 1.0 Ma. The widely cited age of >1.5 Ma derives from a date of 1.51 ± 0.08 Ma (*5*) for a pumice lens lying a few meters above the Grenzbank zone at the base of the Bapang Formation (Fig. 1C, Fig. 2). However, there are other pumice and tuff samples collected from the lowermost part of the Bapang Formation that have produced a group of significantly younger hornblende $^{40}Ar/^{39}Ar$ dates of 0.8–0.9 Ma (*16*, *17*), although one of the samples yielded a date of ca.1.5 Ma which has been provisionally considered to relate to natural reworking (*17*). These 0.8–0.9 Ma dates, centering around 0.88 Ma, are in turn consistent with the newly refined magnetostratigraphy (*18*), which securely establishes the Matuyama-Brunhes polarity transition within the Upper Tuff complex of the Bapang Formation and constrains the age of the uppermost hominin-bearing sediments to ~0.79 Ma. Thus, the controversy over the "long (older)" and "short (younger)" chronologies for the Sangiran hominins is ongoing (*15*, *18*, *23*). Further studies are needed to resolve this issue, and to better understand the biogeographic origins and evolution of Javanese *H. erectus*.

In order to solve this long-standing chronological controversy, we applied a method of combining fission-track and U–Pb dating on zircon grain populations taken from the lowermost Bapang section that directly contains the former sampling location of the $^{40}Ar/^{39}Ar$ 1.51 ± 0.08 Ma (*5*) sample, and also on zircon grains taken from a tuff that could potentially provide a maximum age for the Sangiran hominins. Zircon is commonly observed in volcanic rocks, and is a remarkably robust mineral. The U–Pb zircon method has been recently improved in dating young Quaternary samples (*24*). The U–Pb and fission track methods are directly complementary, because they can be applied to the same zircon grain population. Note that closure temperatures for fission-track and U–Pb chronometry on zircons are ca. 240°C and > 900°C, respectively (*24*). Because zircon variably crystallizes before eruption (*24*), U–Pb ages indicate the timing of crystallization, whereas the fission-track age closely reflects the timing of eruption.

We collected samples for dating from two tephra horizons at the type site of the middle to lower levels of the Bapang Formation near the Bapang Village (columnar section site S48 [Fig. 1B]; fig. S1A, G). Tuff sample BP-LMTCL-1 was collected from the yellowish white tuffaceous sand layer immediately above the Grenzbank zone, whereas pumice sample BP-GB-BC-P1 was taken from the bottom part of the bluish gray clay layer intercalated in the Grenzbank zone (Fig. 2; fig. S1A, B, C, D). We also collected sample Pb-T8 from the yellowish white tuff (Tuff 8) at the V-1 section site (Fig. 1B; fig. S1E, F, G). Tuff 8 is a marked tephra that lies slightly below the base of the Upper Sangiran Formation (Fig. 1C; Fig. 2), that is, stratigraphically underlying the hominin-bearing sediments.

Analytical results are summarized in Fig. 3. Tuff sample BP-LMTCL-1 yielded numerous colorless and euhedral zircon grains that suggest proximal magmatic sources. In order to obtain a robust fission-track date from younger zircons with low spontaneous track density (table S1), we measured > 1600 grains and calculated cumulative grain plateau ages (fig. S2). The weighted mean of two plateau ages was 0.884 ± 0.031 Ma (table S1). As mentioned earlier, it is necessary to consider the time difference of crystallization and eruption. Zircons usually crystallize over an

extended period of time in a magma reservoir, and also individual crystals potentially have various prolonged durations of growth (*24*). The U–Pb age distribution of crystal faces of 75 grains from sample BP-LMTCL-1 is shown in Fig. 3, corresponding to crystallization before and around eruption, with a weighted average age of 0.991 ± 0.005 Ma. The lower tail (younger ages) of the U–Pb age distribution is consistent with the fission-track date of 0.884 ± 0.031 Ma, supporting the interpretation that the lower end of the U–Pb age range approximates the eruption age. These results for the tuff that lies just above the Grenzbank zone demonstrate that the Grenzbank zone is close to 0.9 Ma.

As for the pumice sample BP-GB-BC-P1 taken from within the Grenzbank zone, the number of zircon grains was comparatively fewer, and reliable fission-track dating was not possible. We note that the zircon grains included some reddish detrital ones dated from ~4 Ma to ~90 Ma (*24*). After excluding xenocrystals, weighted averaging of the U–Pb ages from the zircon crystal faces provided a 0.971 ± 0.009 Ma date (Fig. 3). Importantly, the U–Pb age distributions of the two tephra units (BP-GB-BC-P1 and BP-LMTCL-1) correspond well with each other (Fig. 3), suggesting similar crystallization and eruption times, demonstrating that the Grenzbank zone is close to 0.9 Ma. This is consistent with the recently confirmed absence of the Jaramillo subchronozone in the Bapang Formation (*18*), indicating an age younger than 0.99 Ma.

Sample Pb-T8 from Tuff 8, located several meters stratigraphically below the base of the Upper Sangiran Formation (plausible first appearance datum for the Sangiran hominins), yielded zircons suggesting proximal magmatic sources (*24*). Although the number of grains was comparatively fewer, higher spontaneous track density (higher uranium content) allowed reliable fission-track dating, producing a plateau age of 1.345 ± 0.108 Ma (table S1). We consider this date to represent the eruption age of Tuff 8. In our U–Pb dating of the same zircon assemblage, we aimed to estimate a maximum limit of the eruption age, and hence analyzed the inner crystal zones which likely represent preeruptive crystallization regions (*24*). The weighted mean of 1.688 ± 0.010 Ma for the grain U–Pb ages reflects an average timing of crystallization before eruption. The lowermost (youngest) tail of the U–Pb age distribution overlaps with the +2 sigma range (1.56 Ma) of the Tuff 8 fission-track date (Fig. 3), implying that the maximum possible age of Tuff 8 is ~1.55 Ma.

The Grenzbank zone, located at the base of the Bapang Formation, is a key bed of the Sangiran hominin-bearing horizons. The above results for the Grenbank zone (~0.9 Ma) contradict the widely cited bulk hornblende sample $^{40}Ar/^{39}Ar$ date of 1.51 Ma (*5*) for the pumice-rich layer lying a few meters above the Grenzbank zone (Fig. 2), and are consistent with previous $^{40}Ar/^{39}Ar$ determinations, centering around 0.88 Ma, on single hornblende grains (*16, 17*) of pumice/tuff sampled at another locality of the lowermost Bapang Formation. The Larick *et al.*'s (*5*) significantly older $^{40}Ar/^{39}Ar$ date may be provisionally considered to relate to inherited hornblende grains or possible reworking of epiclastic pumice balls.

The majority of the Sangiran hominin fossils were found by chance by local inhabitants, sometimes recovered without precise provenance. Despite this problem, geological and geochemical surveys (*8, 19, 20*), as mentioned earlier, have shown that the hominin specimens could derive from sediments between the Upper Tuff of the Bapang Formation and the upper part of the Sangiran Formation (Fig. 1C). The Sangiran *H. erectus* materials, hitherto variously referred to as *Pithecanthropus* and *Meganthropus*, are tentatively divided into chronologically older and younger groups in light of paleontologic and stratigraphic contexts (*8, 25–27*).

The chronologically younger group includes crania *Pithecanthropus* III (Sangiran 3), VI (Sangiran 10), VII (Sangiran 12) and VIII (Sangiran 17), Skull IX, and mandibles Sb 8103 and Ng 8503. This group is derived from the Bapang Formation above the Grenzbank zone, mainly from sediments near the Middle Tuff (Fig. 1C) (*8, 19*), and is associated with the Kedung Brubus fauna (*25*). Currently, the uppermost datum of the Sangiran hominin fossils has been stratigraphically placed at just below the Upper Middle Tuff (*18*) (Fig. 2); this stratigraphic level lies a few meters below the Matuyama-Brunhes transition and is dated to about 0.79 Ma (*18*).

The chronologically older group includes crania *Pithecanthropus* II (Sangiran 2) and IV (Sangiran 4), crania Sangiran 27 and 31, frontal Bp 9408, maxilla Bpg 2001.04, mandibles *Pithecanthropus* B (Sangiran 1b), C (Sangiran 9) and F (Sangiran 22), mandibles Bk7905 and Bk8606, and mandible *Meganthropus* B (Sangiran 8). The provenience of this group, based on hominin remains with known stratigraphic positions, ranges from the Grenzbank zone (the basal layer of the Bapang Formation, now dated to ~0.9 Ma) to Tuff 11 of the uppermost Sangiran Formation, but plausibly goes down to lower levels in the Upper Sangiran Formation (*8, 19, 20*). This group is associated with the Trinil H.K. fauna and the Ci Saat fauna (*25*) (Fig. 1C). Magnetostratigraphy (*10, 18*) has suggested that the Jaramillo subchronozone lies in the uppermost Sangiran Formation with the lower boundary of the zone (1.07 Ma) near Tuff 11. We estimate the base of the Upper Sangiran Formation, that is, the plausible first appearance datum (FAD) for the Sangiran hominins [*20*], as follows. Using the chronological brackets of 0.884 Ma (the tuff immediately overlying the Grenbank zone) and 1.345 Ma (Tuff 8), the base of the Upper Sangiran Formation (Fig. 1C; Fig. 2) is estimated to be 1.27 Ma, assuming constant depositional rate during this stratigraphic interval. This age estimate is also concordant to the stratigraphic position of Tuff 8 relative to the age of the Lower Lahar lying at the basal Sangiran Formation (Fig. 1C). The latter has been dated at ca. 1.7 Ma by $^{40}Ar/^{39}Ar$ dating of single hornblende grains (*22*), or ca. 1.9 Ma by $^{40}Ar/^{39}Ar$ dating of bulk sample hornblendes (*28*). Considering that the maximum possible age of Tuff 8 is ~1.55 Ma, the FAD for the Sangiran hominins is best considered either ca. 1.27 Ma or < 1.45 Ma.

Some consequences of the short chronology supported here include paleoenvironmental context that relate to adaptation and evolution of Javanese *Homo erectus*. The Sangiran hominins have been shown to comprise two morphologically distinguishable groups, in mandibular, dental and cranial morphology (*23, 26, 27*), with the top of the Grenzbank zone being the stratigraphic and temporal boundary. The older hominin group, although highly variable, displays relatively primitive features that are comparable in morphology to the 1.4–1.7 Ma African *H. erectus* (*H. ergaster*) (*27*). The younger hominin group is comparatively advanced showing a larger neurocranial size and a degree of dentognathic reduction comparable to Middle Pleistocene Chinese *H. erectus* (*23*).

It is well known that the global climate underwent a fundamental change between ca. 1.2 and 0.7 Ma, the mid-Pleistocene transition (MPT), when there was a shift from low-amplitude 41-kyr (thousand years) to high-amplitude 100-kyr climate cycles accompanied by more intensive global glaciation and exposure of continental shelf (*29, 30*). The MPT is characterized by the first major cooling phase at about 900 kyr ago, associated with a rapid increase in global ice volume in marine isotope stage (MIS) 22 (*29, 30*), initiating successive major glaciations. These climatic dynamics profoundly affected the biota and environment. Our estimated age of the Grenzbank zone is approximately at the onset of MIS 22 (ca. 900–866 kyr ago). It is then possible that the morphological changes observed between the older and younger Sangiran

hominin assemblages are associated with some drastic change induced by MIS 22. While *in situ* dynamic microevolution within the same *H. erectus* population is conceivable (*23*), a new immigration event might have been the dominant source of the observed morphological changes. MIS 22 marks the first time in the Pleistocene that the sea level dropped ~120 m below the present level (*30*), and exposed the Sunda shelf around the Indonesian archipelago more widely than before, forming a large landmass. The Kedung Brubus fauna, associated with the younger group of Sangiran hominins, suggests massive interchange with the Asian continent (*25*). To the contrary, the Ci Saat and Trinil H.K. faunae associated with the older hominin group are more insular in character albeit indicating some connection with the mainland.

Concerning the FAD of *H. erectus* in the Sangiran area, our results provide a probable FAD of ~1.3 Ma, and a maximum possible FAD of ~1.45 Ma. Another hominin specimen that have been contended to be the earliest Javanese *H. erectus* is the Mojokerto skull from the Perning site in East Java. This skull is now concluded to be less than ~1.49 Ma based on fission-track age determinations (*31*). Thus, hominin dispersals into Java is resolved to be less than 1.5 Ma. The comparative primitive morphology of the Javanese *H. erectus* of the older chronological group may represent either primitive retentions (*27*) or derived features independently acquired in this hominin lineage.

In conclusion, our results provide important evidence that supports the short (younger) chronology. The Grenzbank zone is securely anchored at ~0.9 Ma and our best estimate for the first hominin colonization into the Sangiran area is ~1.3 Ma (or < 1.5 Ma), both much later than widely accepted for over two decades.

References and Notes:

1. B. Wood, Did early *Homo* migrate "out of" or "in to" Africa? *Proc. Natl Acad. Sci. USA* **108**, 10375–10376 (2011).
2. S. C. Antón, Early *Homo*: Who, when, and where. *Current Anthropology* **53**, Supplement **6**, S278–S298 (2012).
3. G. P. Rightmire, M. S. Ponce de León, D. Lordkipanidze, A. Margvelashvili, C. P. E. Zollikofer, Skull 5 from Dmanisi: Descriptive anatomy, comparative studies, and evolutionary significance. *J. Hum. Evol.* **104**: 50-79 (2017).
4. C. C. Swisher III *et al.* Age of the earliest known hominids in Java, Indonesia. *Science* **263**, 1118–1121 (1994).
5. R. Larick *et al.*, Early Pleistocene $^{40}Ar/^{39}Ar$ ages for Bapang Formation hominins, Central Java, Indonesia. *Proc. Natl Acad. Sci. USA* **98**, 4866–4871 (2001).
6. R. X. Zhu *et al.*, Early evidence of the genus *Homo* in East Asia. *J. Hum. Evol.* **55**, 1075–1085 (2008).
7. H. Tu, G. Shen, D. Granger, X. Yang, Z. Lai, Isochron $^{26}Al/^{10}Be$ burial dating of the Lantian hominin site at Gongwangling in Northwestern China. *Quaternary Geochronol.* **41**, 174–179 (2017).
8. S. Matsu'ura, A chronological framing for the Sangiran hominids; fundamental study by the fluorine dating method. *Bull. Natl Sci. Mus., Tokyo, Ser. D* **8**,1–53 (1982).

9. G. G. Pope, J. E. Cronin, The Asian Hominidae. *J. Hum. Evol.* **13**, 377-396 (1984).

10. M. Hyodo, N. Watanabe, W. Sunata, E. E. Susanto, H. Wahyono, Magnetostratigraphy of hominid fossil bearing formations in Sangiran and Mojokerto, Java. *Anthropol. Sci.* **101**, 157–186 (1993).

11. M. Hyodo *et al.*, Paleomagnetic dates of hominid remains from Yuanmou, China, and other Asian sites. *J. Hum. Evol.* **42**, 27–41 (2002).

12. R. Dennell, in *Out of Africa I: The First Hominin Colonization of Eurasia*, J. G. Fleagle, J. J. Shea, F. E. Grine, A. L. Baden, R. E. Leakey, Eds. (Springer, Dordrecht, 2010), pp. 247–273.

13. S. C. Antón, R. Potts, L. C. Aiello, Evolution of early *Homo*: an integrated biological perspective. *Science* **345**, 1236828 (2014).

14. R. L. Ciochon, E. A. Bettis III, Asian *Homo erectus* converges in time. *Nature* **458**, 153–154 (2009).

15. Y. Zaim *et al.*, New 1.5 million-year-old *Homo erectus* maxilla from Sangiran (Central Java, Indonesia). *J. Hum. Evol.* **61**, 363–376 (2011).

16. H. Saleki *et al.*, Datations radiométriques des couches à *Homo erectus* de Kabuh à Ngebung (Sangiran, Java central, Indonésie). *Actes du XIIIe Congrès UISPP Forli Italie* **2**, 63–74 (1998).

17. C. Falguères *et al.*, Geochronology of early human settlements in Java: What is at stake? *Quaternary Int.* **416**, 5–11 (2016).

18. M. Hyodo *et al.*, High-resolution record of the Matuyama–Brunhes transition constrains the age of Javanese *Homo erectus* in the Sangiran dome, Indonesia. *Proc. Natl Acad. Sci. USA* **108**, 19563–19568 (2011).

19. N. Watanabe, D. Kadar, Eds., *Quaternary Geology of the Hominid Fossil Bearing Formations in Java* (Geological Research and Development Centre, Bandung, 1985).

20. B. Brasseur, F. Sémah, A-M. Sémah, T. Djubiantono, Pedo-sedimentary dynamics of the Sangiran dome hominid bearing layers (Early to Middle Pleistocene, central Java, Indonesia): A palaeopedological approach for reconstructing ‘Pithecanthropus’ (Javanese *Homo erectus*) palaeoenvironment. *Quaternary Int.*, **376**, 84–100 (2015).

21. J. de Vos, P. Y. Sondaar, Dating hominid sites in Indonesia. *Science* **266**, 1726 (1994).

22. F. Sémah, H. Saleki, C. Falguères, G. Féraud, T. Djubiantono, Did Early Man reach Java during the Late Pliocene? *J. Archaeol. Sci.* **27**, 763–769 (2000).

23. Y. Kaifu, F. Aziz, H. Baba, in *Homo erectus in Indonesia: Recent Progress of the Study and Current Understanding*, F. Aziz, H. Baba, Eds. (Centre for Geological Survey, Bandung, 2013), pp. 43–64.

24. Materials and methods are available as supplementary materials.

25. J. de Vos, P. Y. Sondaar, G. D. van den Bergh, F. Aziz, The *Homo* bearing deposits of Java and its ecological context. *Cour. Forsch.-Inst. Senk.* **171**, 129–40 (1994).

26. Y. Kaifu *et al.*, Taxonomic affinities and evolutionary history of the Early Pleistocene hominids of Java: dento-gnathic evidence. *Am. J. Phys. Anthropol.* **128**, 709–726 (2005).

27. Y. Kaifu, E. Indriati, F. Aziz, I. Kurniawan, H. Baba, in *Asian paleoanthropology: from Africa to China and beyond*, C. J. Norton, D. R. Braun, Eds. (Dordrecht, Springer, 2010), pp. 143–157.

28. E. A. Bettis III *et al.*, Landscape development preceding *Homo erectus* immigration into Central Java, Indonesia: the Sangiran Formation Lower Lahar. *Palaeogeogr. Palaeoclim. Palaeoeco.* **206**, 115–131 (2004).

29. P. U. Clark *et al.*, The middle Pleistocene transition: characteristics, mechanisms, and implications for long-term changes in atmospheric pCO_2. *Quaternary Sci. Rev.* **25**, 3150–3184 (2006).

30. H. Elderfield *et al.*, Evolution of ocean temperature and ice volume through the mid-Pleistocene climate transition. *Science* **337**, 704–709 (2012).

31. M. J. Morwood, P. O'Sullivan, E. E. Susanto, F. Aziz, Revised age for Mojokerto 1, an early *Homo erectus* cranium from East Java, Indonesia. *Aust. Archaeol.* **57**, 1–4 (2003).

32. B. Brasseur, *Dynamique et histoire des dépôts du Pléistocène inférieur et moyen ancien dans le dôme de Sangiran (Java central, Indonésie)* (Ph.D. thesis. Département de Préhistoire, Muséum national d'Histoire naturelle, 2009).

33. T. Danhara, T. Yamashita, H. Iwano, M. Kasuya, An improved system for measuring refractive index using the thermal immersion method. *Quaternary Int.* **13/14**, 89–91 (1992).

34. R. L. Fleischer, P. B. Price, R. M. Walker, *Nuclear Tracks in Solids: Principles and Applications* (University of California Press, 1975).

35. G. A. Wagner, P. Van den Haute, *Fission-Track Dating* (Enke, Stuttgart, 1992).

36. A. J. W. Gleadow, Fission-track dating methods: what are the real alternatives? *Nucl. Tracks* **5**, 3–14 (1981).

37. T. Tsuruta, Characteristics of diallyl phthalate resin as a fission track detector. *Radiat. Meas.* **31**, 99–102 (1999).

38. T. Danhara, M. Kasuya, H. Iwano, T. Yamashita, Fission-track age calibration using internal and external surfaces of zircon. *J. Geol. Soc. Japan* **97**, 977–985 (1991).

39. T. Yoshioka, T. Tsuruta, H. Iwano, T. Danhara, Y. Koguchi, Fission-fragment registration and etching properties of diallyl phthalate with reference to its use as an external detector in fission track dating. *Nucl. Instr. Meth. Phys. Res.* B **207**, 323–332 (2003).

40. T. Danhara, H. Iwano, T. Yoshioka, T. Tsuruta, Zeta calibration values for fission track dating with a diallyl phthalate detector. *J. Geol. Soc. Japan* **109**, 665–668 (2003).

41. A. J. Hurford, P. F. Green, A users' guide to fission track dating calibration. *Earth Planet. Sci. Lett.* **59**, 343–354 (1982).

42. A. J. Hurford, Standardization of fission track dating calibration: recommendation by the Fission Track Working Group of the I.U.G.S. Subcommission of Geochronology. *Chem. Geol. (Isot. Geosci. Sect.)* **80**, 171–178 (1990).

43. A. J. Hurford, R. T. Watkins, Fission-track age of the tuffs of the Buluk Member, Bakate Formation, northern Kenya: a suitable fission-track age standard. *Chem. Geol. (Isot. Geosci. Sect.)* **66**, 209–216 (1987).

44. A. J. Hurford, K. Hammerschmidt, $^{40}Ar/^{39}Ar$ and K/Ar dating of the Bishop and Fish Canyon Tuffs: Calibration ages for fission-track dating standards. *Chem. Geol. (Isot. Geosci. Sect.)* **58**, 23–32 (1985).

45. A. J. Hurford, P. F. Green, The zeta age calibration of fission-track dating. *Isot. Geosci.* **1**, 285–317 (1983).

46. T. Danhara, H. Iwano, A review of the present state of the absolute calibration for zircon fission track geochronology using the external detector method. *Island Arc* **22**, 264–279 (2013).

47. H. Iwano, T. Danhara, T. Hirata, Standardless fission-track ages of the IUGS age-standards. *Chem. Geol.* doi.org/10.1016/j.chemgeo.2018.04.011 (2018).

48. D. J. Cherniak, E. B. Watson, Pb diffusion in zircon. *Chem. Geol.* **172**, 5–24 (2001).

49. A. J. Hurford, Cooling and uplift patterns in the Lepontine Alps South Central Switzerland and an age of vertical movement on the Insubric fault line. *Contrib. Mineral. Petr.* **92**, 413–427 (1986).

50. M. D. Schmitz, S. A. Bowring, U–Pb zircon and titanite systematics of the Fish Canyon Tuff: an assessment of high-precision U–Pb geochronology and its application to young volcanic rocks. *Geochim. Cosmochim. Acta* **65**, 2571–2587 (2001).

51. P. R. Renne, R. Mundil, G. Balco, K. Min, K. R. Ludwig, Joint determination of ^{40}K decay constants and $^{40}Ar^*/^{40}K$ for the Fish Canyon sanidine standard, and improved accuracy for $^{40}Ar/^{39}Ar$ geochronology. *Geochim. Cosmochim. Acta* **74**, 5349–5367 (2010).

52. M. Ganerød *et al.*, Geochronology of the Tardree Rhyolite Complex, Northern Ireland: Implications for zircon fission track studies, the North Atlantic Igneous Province and the age of the Fish Canyon sanidine standard. *Chem. Geol.* **286**, 222–228 (2011).

53. S. Sakata *et al.*, Determination of U–Pb ages for young zircons using laser ablation-ICP-mass spectrometry coupled with an ion detection attenuator device. *Geostandards and Geoanaly. Res.* **38**, 409–420 (2014).

54. K. F. Kuiper *et al.*, Synchronizing rock clocks of Earth history. *Science* **320**, 500–504 (2008).

55. F. M. Gradstein, J. G. Ogg, M. Schmitz, G. Ogg, *The Geologic Time Scale 2012* (Elsevier, 2012).

56. A. Gleadow, M. Harrison, B. Kohn, R. Lugo-Zazueta, D. Phillips, The Fish Canyon Tuff: A new look at an old low-temperature thermochronology standard. *Earth Planet. Sci. Lett.* **424**, 95–108 (2015).

57. T. Danhara, H. Iwano, A report on fission-track data of zircon and apatite age-standard for age calibration using diallyl phthalate (DAP) resin detectors and a minor revision of zeta values by Danhara *et al.* (2003). *J. Geol. Soc. Japan* **113**, 77–81 (2007).

58. D. Seward, B. P. Kohn, New zircon fission-track ages from New Zealand Quaternary tephra: an interlaboratory experiment and recommendations for the determination of young ages. *Chem. Geol.* **141**, 127–140 (1997).

59. H. Takagi, K. Arita, T. Danhara, H. Iwano, Timing of the Tsergo Ri landslide, Langtang Himal, determined by fission-track dating of pseudotachylyte. *J. Asian Earth Sci.* **29**, 466–472 (2007).

60. A. K. Schmitt *et al.*, The Geysers - Cobb Mountain Magma System, California (Part 1): U–Pb zircon ages of volcanic rocks, conditions of zircon crystallization and magma residence times. *Geochim. Cosmochim. Acta* **67**, 3423–3442 (2003).

61. J. L. Crowley, B. Schoene, S. A. Bowring, U–Pb dating of zircon in the Bishop Tuff at the millennial scale. *Geology* **35**, 1123–1126 (2007).

62. J. I. Simon, P. R. Renne, R. Mundil, Implications of pre-eruptive magmatic histories of zircons for U–Pb geochronology of silicic extrusions. *Earth Planet. Sci. Lett.* **266**, 182–194 (2008).

63. M. Guillong, A. von Quadt, S. Sakata, I. Peytcheva, O. Bachmann, LA-ICP-MS Pb–U dating of young zircons from the Kos–Nisyros volcanic centre, SE Aegean arc. *J. Anal. At. Spectrom.* **29**, 963–970 (2014).

64. S. Sakata *et al.*, A new approach for constraining the magnitude of initial disequilibrium in Quaternary zircons by coupled uranium and thorium decay series dating. *Quaternary Geochronol.* **38**, 1–12 (2017).

65. A. Tunheng, T. Hirata, Development of signal smoothing device for precise elemental analysis using laser ablation-ICP-mass spectrometry. *J. Anal. Atom. Spectrom.* **19**, 932–934 (2004).

66. N. E. Matthews, J. A. Vazquez, A. T. Calvert, Age of the Lava Creek supereruption and magma chamber assembly from combined $^{40}Ar/^{39}Ar$ and U–Pb dating of sanidine and zircon crystals. *Geochem. Geophys. Geosys.***16**, 2508–2528 (2015).

67. A. K. Schmitt, Uranium series accessory crystal dating of magmatic processes. *Ann. Rev. Earth Pl. Sci.* **39**, 321–349 (2011).

68. T. Iizuka, T. Hirata, Simultaneous determinations of U–Pb and REE abundances for zircons using ArF excimer laser ablation-ICPMS. *Geochem. J.* **38**, 229–241 (2004).

69. K. Hattori, S. Sakata, M. Tanaka, Y. Orihashi, T. Hirata, U–Pb age determination for zircons using a laser ablation-ICP-mass spectrometry equipped with six multiple-ion counting detectors. *J. Anal. At. Spectrom.* **32**, 88–95 (2017).

70. J. Hiess, D. J. Condon, N. McLean, S. R. Noble, $^{238}U/^{235}U$ Systematics in terrestrial uranium-bearing minerals. *Science* **335**, 1610–1614 (2012).

71. A. H. Jaffey, K. F. Flynn, L. E. Glendenin, W. C. Bentleyt, A. M. Essling, Precision measurement of half-lives and specific activities of ^{235}U and ^{238}U. *Phys. Rev. C* **4**, 1889–1906 (1971).

72. M. Wiedenbeck *et al.*, Three natural zircon standards for U–Th–Pb, Lu–Hf, trace element and REE analyses. *Geostandards Newslet.* **19**, 1–23 (1995).

73. M. R. Reid, C. D. Coath, T. M. Harrison, K. D. McKeegan, Prolonged residence times for the youngest rhyolites associated with Long Valley Caldera: $^{230}Th–^{238}U$ ion microprobe dating of young zircons. *Earth Planet. Sci. Lett.* **150**, 27–39 (1997).

74. K. P. Jochum, B. Stoll, in *Laser Ablation ICP-MS in the Earth Sciences: Current Practices and Outstanding Issues* (ed. Sylvester, P. J.) 147–168 (Mineralogical Association of Canada, 2008).

75. J. Sláma *et al.*, Plešovice zircon — A new natural reference material for U–Pb and Hf isotopic microanalysis. *Chem. Geol.* **249**, 1–35 (2008).

76. H. Iwano *et al.*, An inter-laboratory evaluation of OD-3 zircon for use as a secondary U–Pb dating standard. *Isl. Arc* **22**, 382–394 (2013).

77. R. Lukács *et al.*, Zircon geochronology and geochemistry to constrain the youngest eruption events and magma evolution of the Mid-Miocene ignimbrite flare-up in the Pannonian Basin, eastern central Europe. *Contrib. Mineral. Petr.* **170**, 52 (2015).

78. J. M. Mattinson, Anomalous isotopic composition of lead in young zircons. *Carnegie Inst. Wash. Year Book* **72**, 613–616 (1973).

79. K. R. Ludwig, Effect of initial radioactive-daughter disequilibrium on U–Pb isotope apparent ages of young minerals. *J. Res. U.S. Geol. Surv.* **5**, 663–667 (1977).

80. U. Schärer, The effect of initial ^{230}Th disequilibrium on young U–Pb ages: the Makalu case, Himalaya. *Earth Planet. Sci. Lett.* **67**, 191–204 (1984).

81. I. Wendt, C. Carl, U–Pb dating of discordant 0.1 Ma old secondary U minerals. *Earth Planet. Sci. Lett.* **73**, 278–284 (1985).

82. S. Sakata, A practical method for calculating the U–Pb age of Quaternary zircon: correction for common Pb and initial disequilibria. *Geochem. J.* **52**, 281–286 (2018).

83. N. J. G. Pearce *et al.*, A compilation of new and published major and trace element data for NIST SRM 610 and NIST SRM 612 glass reference materials. *Geost. Newslet.* **21**, 115–144 (1997).

84. M. Rioux, S. Bowring, M. Cheadle, B. John, Evidence for initial excess ^{231}Pa in mid-ocean ridge zircons. *Chem. Geol.* **397**, 143–156 (2015).

85. J. S. Stacey, J. D. Kramers, Approximation of terrestrial lead isotope evolution by a two-stage model. *Earth Planet. Sci. Lett.* **26**, 207–221 (1975).

86. K. R. Ludwig, Isoplot/Ex ver. 3.00: a geochronological tool kit for Microsoft Excel. *Berkeley Geochronol. Center Spec. Publ.* **4**, 71 (2003).

87. J. I. Simon *et al.*, Accessory mineral U–Th–Pb ages and ^{40}Ar/^{39}Ar eruption chronology, and their bearing on rhyolitic magma evolution in the Pleistocene Coso volcanic field, California. *Contrib. Mineral. Petrol.* **158**, 421–446 (2009).

88. R. F. Galbraith, On statistical models for fission track counts. *J. Math. Geol.* **13**, 471–478 (1981).

ACKNOWLEDGMENTS

This chronological research was done under the auspices of the Centre for Geological Survey (CGS: formerly Geological Research and Development Centre), Bandung, Indonesia. We thank the successive directors of CGS for continued support and courtesy lasting more than a quarter of

a century. This joint research project was conducted partly under the general agreement of cooperation between CGS and the National Museum of Nature and Science, Tokyo (NMNS). We thank H. Baba and Y. Kaifu of NMNS for consideration and help. Special thanks are due to the late Sudijono of CGS for long-term collaboration since the 1970s. We owe a very important debt to the late H. Kumai of Osaka City University, without whose enormous amount of work and instruction this project would not have been possible. We are also grateful to N. Watanabe (deceased) and D. Kadar, who made a beginning of Indonesia-Japan research cooperation in this field. **Funding:** This study was partially supported by the Japan Society for the Promotion of Science (Grant nos.13440255, 15403015, 18200053, 22320154) and by NMNS (Fund no. 6503).
Author Contributions: S.M. and F.A. planned and coordinated the original chronological project with I. Kurniawan, M.H. and M.K.; this dating analyses were planned by T.D., T.H. and S.M.; F.A., I. Kurniawan, M.H., M.K., Y.T., E.S., I. Kitaba., H.I., S.S., T.D., T.H., M.S., Y.D. and S.M. performed research; T.D., H.I., S.S., M.K., Y.D., T.H. and M.S. undertook dating experiments; S.M. prepared the manuscript, with input from H.I., S.S., T.D., Y.T. and M.H. including tables and figures, and additional contributions from other authors. **Competing interests:** The authors declare no competing financial interests. **Data and materials availability:** The data that support the findings of this study are available in the paper and supplementary materials.

Supplementary Materials:

Materials and Methods

Figs. S1–S5

Tables S1–S5

References (*33–88*)

Fig. 1. Location of Sangiran (A), geological map (B) and generalized stratigraphy (C) of the Sangiran area (after refs *19, 20, 25, 32*). In **B**, a thick red arrow (S48) and a short red line (V-1) show the columnar section localities involved with samples for dating. Crosses show *Homo erectus* fossil sites; some of them are indicated with registered designation: mandible *Pithecanthropus* B (Pb), mandible *Pithecanthropus* C (Pc), mandible *Pithecanthropus* E (Pe), mandible *Pithecanthropus* F (Pf), mandible *Meganthropus* B (Mb), calotte *Pithecanthropus* II (P II), calotte *Pithecanthropus* III (P III), cranium *Pithecanthropus* IV (P IV), calotte *Pithecanthropus* VI (P VI), calotte *Pithecanthropus* VII (P VII), and cranium *Pithecanthropus* VIII (P VIII).

Fig. 2. Geological columnar sections showing the stratigraphic levels of the tephra samples treated in this study (BP-LMTCL-1, BP-GB-BC-P1 and Pb-T8). For the locations and photographs of the sampling sites, see fig. S1. Note that the U–Pb age represents an average of timing of zircon crystallization which commonly occurs significantly before eruption, and that the deposition time of the unit layer is younger than the U–Pb age (*24*; see Fig. 3).

Fig. 3. Zircon fission track age for BP-LMTCL-1 and Pb-T8 (see Table S1) and the U–Pb age results of zircon grains for BP-LMTCL-1, BP-GB-BC-P1 and Pb-T8 (data in Table S5). The closure temperature (ca. 240°C) of zircon fission track chronometry is much lower than that

(> 900°C,) of U–Pb systematics. The weighted mean of grain U–Pb ages signifies an average of timing of crystallization which variably occurs before eruption (*24*), where the fission-track date should represent the eruption age. Note that the 2σ ranges of the weighted mean U–Pb ages of BP-LMTCL-1 and BP-GB-BC-P1 considerably overlap, and the two groups of grain U–Pb ages show statistically comparable overall crystallization distributions (P=0. 483, two-sample K–S test, two-side).

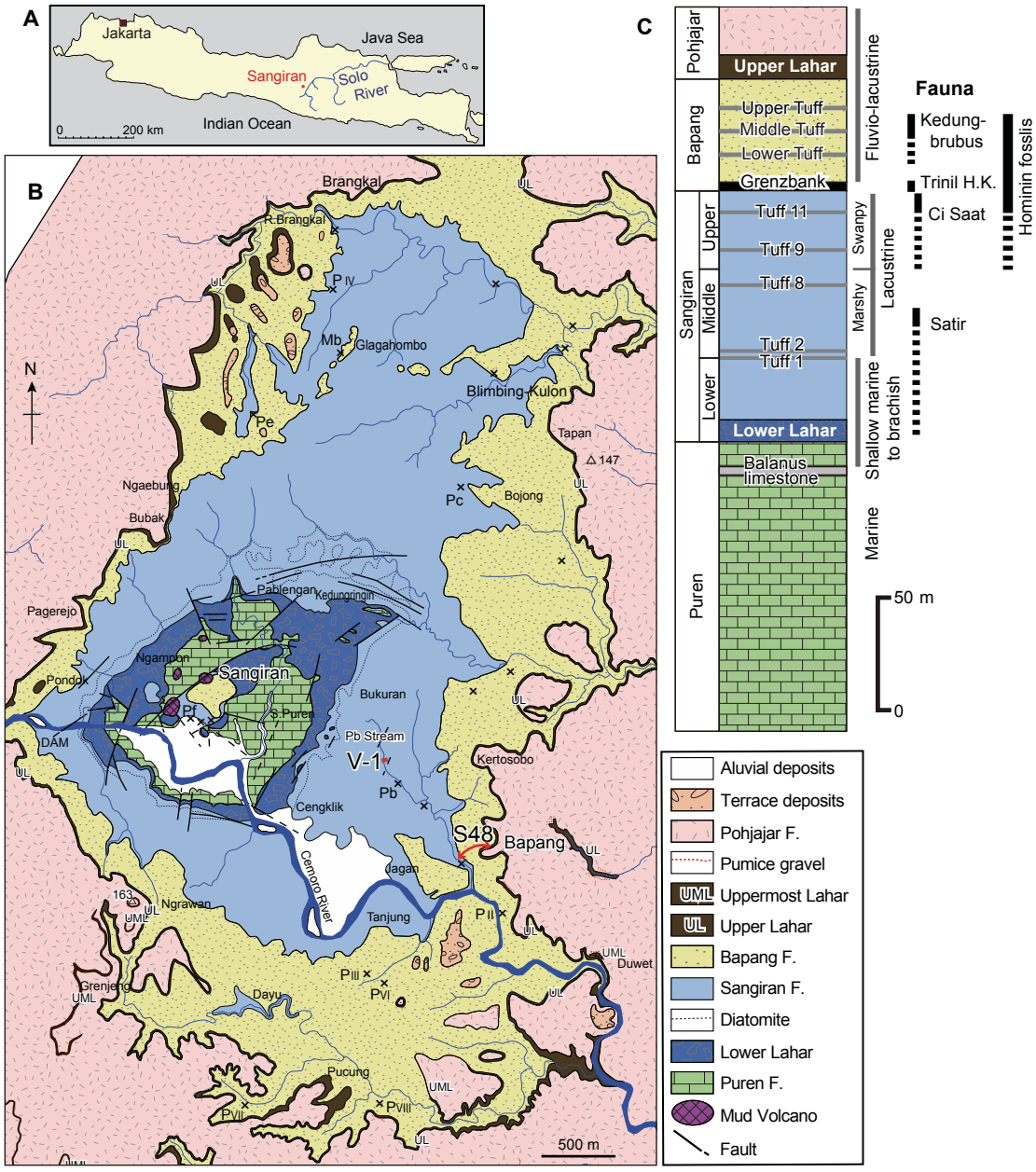
A
Jakarta
Java Sea
Sangiran
Solo River
Indian Ocean
0
200 km
B
Brangkal
R.Brangkal
P IV
Mb
Glagahombo
Blimbing
Kulon
Pe
Tapan
△147
Pc
Bojong
Ngaebung
Bubak
Pablengan
Kedungringin
Pagerejo
Ngampon
Sangiran
Pondok
Pf
S. Puren
Bukuran
Pb Stream
V-1
Pb
DAM
Kertosobo
Cengklik
S48
Bapang
Jagan
Cemoro River
163
Ngrawan
Tanjung
P II
Duwet
Grenjeng
P III
P VI
Dayu
Pucung
P VII
P VIII
500 m
N
C
Pohjajar
Upper Lahar
Bapang
Upper Tuff
Middle Tuff
Lower Tuff
Grenzbank
Sangiran
Upper
Middle
Lower
Tuff 11
Tuff 9
Tuff 8
Tuff 2
Tuff 1
Lower Lahar
Puren
Balanus limestone
Fluvio-lacustrine
Swanpy
Marshy
Lacustrine
Shallow marine to brachish
Marine
50 m
0
Fauna
Kedung-brubus
Trinil H.K.
Ci Saat
Satir
Hominin fosslis
Aluvial deposits
Terrace deposits
Pohjajar F.
Pumice gravel
Uppermost Lahar
Upper Lahar
Bapang F.
Sangiran F.
Diatomite
Lower Lahar
Puren F.
Mud Volcano
Fault

Fig. 1

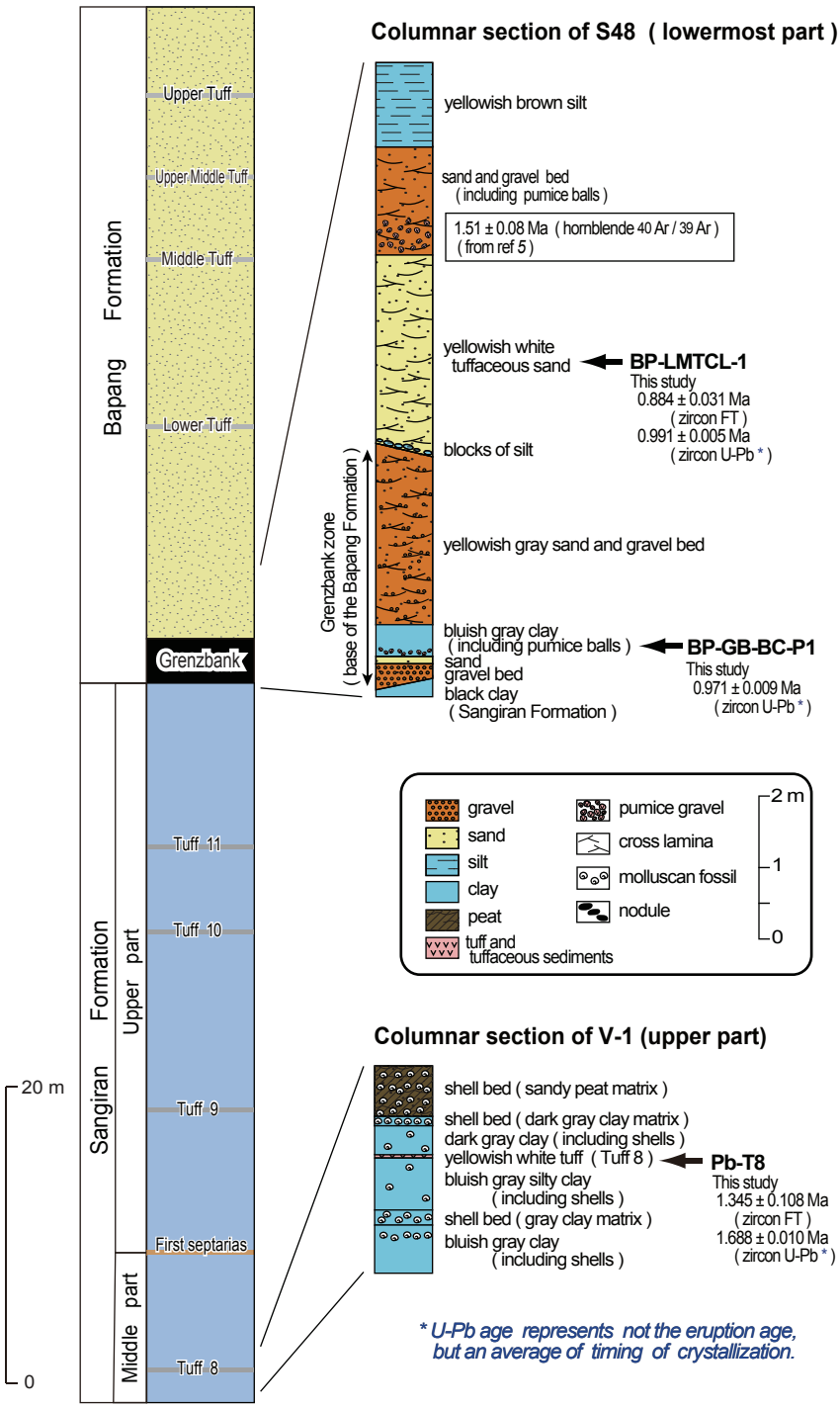
Columnar section of S48 (lowermost part)
Bapang Formation
Upper Tuff
Upper Middle Tuff
Middle Tuff
Lower Tuff
Grenzbank
Grenzbank zone
(base of the Bapang Formation)
yellowish brown silt
sand and gravel bed
(including pumice balls)
1.51 ± 0.08 Ma (hornblende 40 Ar / 39 Ar)
(from ref 5)
yellowish white
tuffaceous sand
BP-LMTCL-1
This study
0.884 ± 0.031 Ma
(zircon FT)
0.991 ± 0.005 Ma
(zircon U-Pb *)
blocks of silt
yellowish gray sand and gravel bed
bluish gray clay
(including pumice balls)
sand
gravel bed
black clay
(Sangiran Formation)
BP-GB-BC-P1
This study
0.971 ± 0.009 Ma
(zircon U-Pb *)
Sangiran Formation
Upper part
Middle part
Tuff 11
Tuff 10
Tuff 9
First septarias
Tuff 8
20 m
0
gravel
sand
silt
clay
peat
tuff and
tuffaceous sediments
pumice gravel
cross lamina
molluscan fossil
nodule
2 m
1
0
Columnar section of V-1 (upper part)
shell bed (sandy peat matrix)
shell bed (dark gray clay matrix)
dark gray clay (including shells)
yellowish white tuff (Tuff 8)
Pb-T8
This study
1.345 ± 0.108 Ma
(zircon FT)
1.688 ± 0.010 Ma
(zircon U-Pb *)
bluish gray silty clay
(including shells)
shell bed (gray clay matrix)
bluish gray clay
(including shells)
* U-Pb age represents not the eruption age,
but an average of timing of crystallization.

Fig. 2

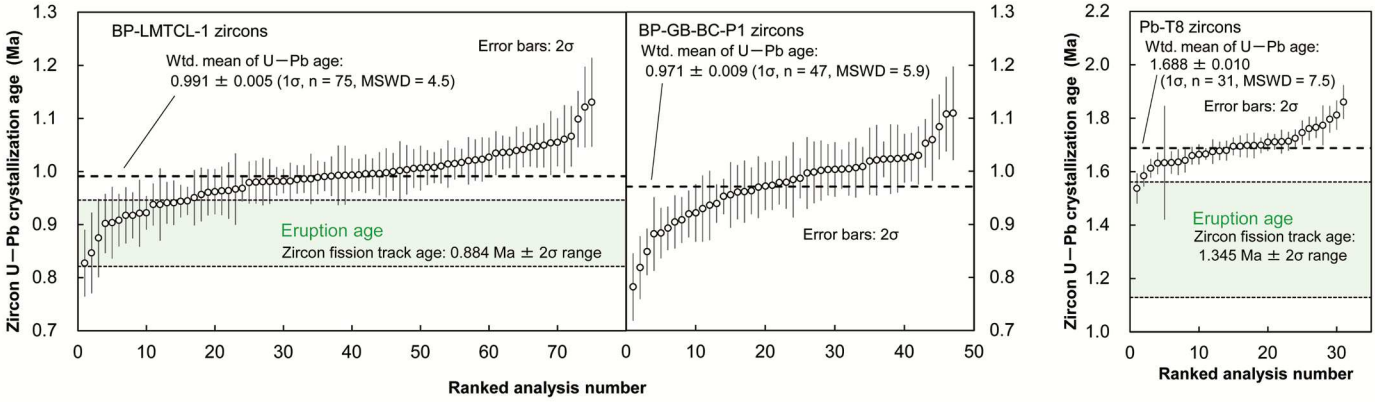
BP-LMTCL-1 zircons
Wtd. mean of U—Pb age:
0.991 ± 0.005 (1σ, n = 75, MSWD = 4.5)
Error bars: 2σ
Eruption age
Zircon fission track age: 0.884 Ma ± 2σ range
BP-GB-BC-P1 zircons
Wtd. mean of U—Pb age:
0.971 ± 0.009 (1σ, n = 47, MSWD = 5.9)
Error bars: 2σ
Pb-T8 zircons
Wtd. mean of U—Pb age:
1.688 ± 0.010
(1σ, n = 31, MSWD = 7.5)
Error bars: 2σ
Eruption age
Zircon fission track age:
1.345 Ma ± 2σ range
Zircon U—Pb crystallization age (Ma)
Ranked analysis number

Fig. 3

Science
AAAS

Supplementary Materials for

Age control of the first appearance datum for Javanese *Homo erectus* in the Sangiran area

Shuji Matsu'ura*, Megumi Kondo, Tohru Danhara, Shuhei Sakata, Hideki Iwano, Takafumi Hirata, Iwan Kurniawan, Erick Setiyabudi, Yoshihiro Takeshita, Masayuki Hyodo*, Ikuko Kitaba, Masafumi Sudo, Yugo Danhara, Fachroel Aziz

*Corresponding author. Email: matsu-ur@js2.so-net.ne.jp (S.M); mhyodo@kobe-u.ac.jp (M.H.)

This PDF file includes:

Materials and Methods
Figs. S1 to S5
Tables S1 to S5
References

Materials and Methods

Tephra samples, mineral separation and zircons used in this study

Stratigraphic positions of the tephra samples treated in this study (BP-LMTCL-1, BP-GB-BC-P1 and Pb-T8) are shown in Fig. 2, and locations and photographs of the sampling sites are given in Fig. S1. Tuff sample BP-LMTCL-1 was taken from the yellowish white tuffaceous sand layer with cross lamination (Fig. S1B, C) immediately above the Grenzbank zone. Pumice sample BP-GB-BC-P1 was collected from the bluish gray clay layer (Fig. S1D) in the Grenzbank zone. The pumice balls are 0.2–0.5 cm in diameter, white in color, and so soft that they could be crushed with a finger, but sharply defined, representing a probable flush of new volcaniclastic material. These observations indicate that the pumice has not been extensively reworked. Tuff sample Pb-T8 was taken from the yellowish white tuff of fine to medium sand size (Tuff 8) (Fig. S1F) that lies slightly below the base of the Upper Sangiran Formation. Concerning the sample Pb-T8, this sample was collected at the V-1 section site (Fig. 1B and ref *19*); this V-1 section was included by Yoshikawa and Suminto (in ref *19*) as part of their composite 'Loc. 4' section (composite of V-1 to V-4 columnar sections) (*19*), which contains Tuff 7 to Tuff 11 of the Sangiran Formation. Among them, Tuff 8 occurs in the V-1 section (*19*).

A subsample of each tephra sample was subjected to analyses for mineral assemblage and refractive indices. After washing on a 63-μm sieve and examined under a binocular microscope, the remnant of each sample was then washed on 63-, 125-, and 250-μm mesh sieves. The 63- to 125-μm fraction was mounted on glass slides, and the bulk grain composition and heavy mineral composition were determined under a microscope. Refractive indices of volcanic glass shards (if not weathered) and also plagioclase and hornblende crystals, were measured individually for identification of the dated tephras using a refractive index measurement system (RIMS) analyzer (*33*). Results of the tephra analyses are shown in Fig. S3.

Euhedral zircon grains were collected through heavy-liquid and magnetic mineral separation techniques. The tuff sample BP-LMTCL-1 yielded a large number of colorless and euhedral zircon grains suggesting proximal magmatic sources; they were submitted to fission-track and U–Pb dating. As for the pumice sample BP-GB-BC-P1, zircon grains recovered were fewer in number and smaller in size, and not feasible for the determination of young ages by the fission-track method. Furthermore, the BP-GB-BC-P1 zircon consisted not only of colorless grains (~90%) but also of reddish ones (~10%). Preliminary fission-track and U–Pb dating of the reddish grains revealed that they are detrital with older ages of ~4 Ma (4.3 ± 0.3 [1σ, n = 1, U–Pb] Ma), ~12 Ma (11.9 ± 0.3 [1σ, n = 5, U–Pb] Ma, 13.1 ± 6.6 [1σ, n = 1, FT] Ma), ~17 Ma (17.1 ± 0.5 [1σ, n = 4, U–Pb] Ma, 15.9 ± 2.6 [1σ, n = 3, FT] Ma), ~22 Ma (22.1 ± 1.0 [1σ, n = 3, U–Pb] Ma) and ~90 Ma (91.6 ± 6.0 [1σ, n = 1, U–Pb] Ma, 90.9 ± 28.0 [1σ, n = 1, FT] Ma), all of which were excluded when submitting to the U–Pb dating. These derived grains may be considered to be due to mixing of older zircon crystals into pumice that contains primary zircons. Tuff sample Pb-T8 yielded homogeneous and euhedral grains of pale pinkish zircons, suggesting proximal magmatic sources. Although the number of grains was comparatively fewer, higher uranium content, that is, higher spontaneous fission-track density (Table S1) allowed age determination by the fission-track method. The Pb-T8 zircons were submitted to fission-track and U–Pb dating.

Fission-track dating

Radiometric dating using fission tracks is based on the spontaneous fission decay of ^{238}U atoms (*34, 35*). The age of a mineral sample can be obtained by measuring the spontaneous-track density if the uranium content is known. The existing concentration of uranium is usually determined from track-density measurement of ^{235}U fissions induced by thermal neutron irradiation in a reactor. We here adopt the most widely used external detector method (ED2 method) that applies to external natural surfaces (*36*).

Zircon grains, separated from pumice/tuff samples, were mounted in a PFA Teflon-sheet with external surfaces exposed. The external natural surfaces of zircons were subjected to fission track dating because of easier track identification due to longer track length distribution on the external surface geometry. After chemical etching treatment using an eutectic mixture of KOH and NaOH at 225 °C for 48 h (Indonesian samples) or 24 h (Fish Canyon Tuff standard), enlarged fission tracks were counted under the microscope. This is followed by the counting of induced tracks of ^{235}U in an external detector of uranium-free plastic, diallyl-phthalate (*37*) (DAP), which was set in an intimate contact with the zircon mounts during thermal-neutron irradiations. Track counting was done using a Nikon Biophot microscope with oculars and a 100× dry objective (*38*). NIST-SRM612 standard glass was used as a dosimeter, and irradiated with a thermal neutron fluence of ~ 5×10^{14} n·cm^{-2} together with samples. Two irradiation runs were made in the pneumatic tube of JRR-4 reactor (thermal neutron flux: 3.2×10^{13} n·cm^{-2}·sec^{-1}) unit of the Japan Atomic Energy Agency (JAEA). The cadmium ratio for Au at this position is 3.6. After irradiation, the DAP detectors were detached, and induced tracks were etched in a solution of 15% KOH, 65% ethanol and 20% H_2O at 60 °C for 2 min (*39*). Induced track density measurement for the NIST-SRM612 dosimeter glass was made by using the monitor observation system composed of a Nikon Eclipse E1000 microscope with a 100× dry objective, a Tokyo Electronic Industry HVC7110 TV camera, and a Chuomusen THM-14A video monitor described in Danhara *et al.* (*40*).

The fission-track age is usually calibrated by a standard-based protocol, what is called zeta calibration (*41*) with a zeta factor specific for the counting system of the laboratory. The zeta value of zircon for dating with the DAP detectors was first reported by Danhara *et al.* (*40*), using three age standards recommended by the IUGS Subcommission on Geochronology (*42*): zircons from the Buluk Member Tuff (BMT) with a reference age of 16.3 ± 0.2 (2σ) Ma (*43*), the Fish Canyon Tuff (FCT) with a reference age of 27.8 ± 0.2 (2σ) Ma (*44*), and the Tardree Rhyolite (TR) with a reference age of 58.7 ± 1.1 (2σ) Ma (*45*). The resulting zeta value for the ED2 method is 350 ± 3 based on the above three reference ages determined with the K-Ar or $^{40}Ar/^{39}Ar$ method and cited in the IUGS recommendation. However, with recent efforts to re-establish the absolute calibration for zircon fission-track geochronology (*46*), it has been found that the use of zircon U–Pb ages as reference for the zeta calibration approach is more reasonable when using the current IUGS standard samples (*47*). In this connection, the difference of closure temperatures for zircon between the U–Pb system (> 900 °C) (*48*) and the fission-track system (ca. 240 °C) (*49*) is a matter of concern. These two chronometers are supposed to give the times of crystallization of zircon grains and volcanic eruption, respectively. Iwano *et al.* (*47*) denote a short time interval between crystallization and eruption for those IUGS standard samples. Furthermore, high-precision U–Pb dating applied to young volcanic rocks and refined $^{40}Ar/^{39}Ar$ geochronology with revision of decay constants involved have called for re-evaluation of the commonly accepted ages hitherto for zircon fission track standards (e.g. *50, 51, 52*). Here we revise the zircon zeta value for the ED2 method with the DAP detectors from 350 ± 3 to 356 ± 3 (Table S1), using the following U-Pb zircon ages as reference: 16.1 ± 0.3 (2σ) Ma by the laser-

ablation inductively-coupled plasma mass spectrometry for BMT (newly-obtained by H.I., T.D. and T.H., following the procedure of Sakata *et al.* [*53*]; Table S2), 28.476 ± 0.064 (2σ) Ma by the isotope dilution thermal ionization mass spectrometry (TIMS) for FCT (*50*), and 61.32 ± 0.09 (2σ) Ma by the chemical abrasion TIMS for TR (*52*). As for FCT and TR, although these U–Pb ages are a little older than the reference values formerly used in Danhara *et al.* (*40*), they are consistent with the astronomically calibrated $^{40}Ar/^{39}Ar$ age of FCT sanidine[53] that is cited in The Geologic Time Scale 2012 (*55*), and with results from recent high precision sanidine $^{40}Ar/^{39}Ar$ and apatite (U–Th)/He geochronology (*52, 56*). Our zeta value calculation is based on 20 measurement data on the three IUGS standard samples from 4 irradiations (see *40*). Alternatively, the use of the astronomical tuning age of 28.201 ± 0.046 (2σ) Ma for FCT (*54*) gives a zeta value of 354 ± 3, compatible with that (356 ± 3) used in this study. Using 356 ± 3 gives 1.7 % older date than the use of the previous zeta value of 350 ± 3.

To test reproducibility of the fission-track dating approach described here, the widely used FCT zircon standard was periodically and repeatedly analyzed. Twenty-seven experiments (see *57*) provided a weighted mean of 28.4 ± 0.2 Ma with a sample standard deviation of 1.5 Ma, and all the fission-track age data obtained are found to be within ± 2 SD ranges, showing the reliability of this method.

Due to small number of spontaneous track counts per grain in the case of the young zircons treated in this study, we found it necessary to plot running (moving) means of the single-crystal ages to determine when the final age has been approached (*58, 59*). As shown in Fig. S2, we adopted the pooled age of multi-grains and confirmed that the cumulative moving average made a plateau.

U–Pb dating

The application of U–Pb dating to young Quaternary zircons has been recently improved (*53, 60–64*). In this study, U–Pb isotopic analyses (see Tables S3 and S4) were conducted using a multiple collector inductively-coupled plasma (ICP) mass spectrometer (Nu Plasma II, Nu instruments, Wrexham, UK) coupled to an ArF Excimer laser ablation system (ESI NWR-193, Portland, USA). The laser was operated with a repetition rate of 2 Hz and a spot size of 35 μm. A two-volume cell (ESI, Portland, USA) was used throughout the measurements and ablation was carried out in a He atmosphere, utilizing a small volume cell (< 1 cm^3) to reduce sample washout time. The He carrier gas was mixed with Ar gas outside the ablation cell, and the laser-induced sample particles were carried to the ICP ion source in a mix of He and Ar. A laser fluence of 2.1 Jcm^{-2} was used throughout this study. A signal-smoothing device was also used (*65*).

Several recent studies have reported that the outer rim of zircon crystal tends to show younger U–Pb age than that of interior region in single crystals (*66, 67*), since individual crystals may have various prolonged durations of growth. Hence, the weighted mean of grain U–Pb ages of the external surfaces of zircon crystals reflects an average of timing of crystallization which may occur continuously in a magma reservoir (*63, 67*) before and around eruption, whereas the weighted mean of grain U–Pb ages of inner crystal zones (polished surfaces) would reflect an average of timing of earlier (preeruptive) crystallization in a magma reservoir.

Totally, 50 laser pulses were irradiated for one spot and the depth of the resulting crater is ca. 2.5 μm. Under these conditions, time-dependent elemental or isotopic fractionation of Pb/U and Pb/Pb was insignificant. Pre-cleaning of the analyzed surface of zircons was carried out by a single pre-ablation shot at each analytical site prior to the actual measurements (*68*).

Five full-size electron multipliers were used for the simultaneous detection of ion signals: ^{202}Hg, ^{204}(Hg + Pb), ^{207}Pb, ^{208}Pb, and ^{235}U. Signal intensities of ^{206}Pb and ^{232}Th were monitored using a Daly collector and a Faraday collector, respectively (laser ablation multiple collector ICP-MS: LA-MC-ICP-MS). Dead times of electron multipliers and a Daly collector were calibrated similar to that described in Hattori *et al.* (*69*). Recently, Hiess *et al.* (*70*) reported heterogeneity of ^{238}U/^{235}U for terrestrial uranium-bearing minerals. This variation in ^{238}U/^{235}U is much smaller than the uncertainties in isotopic analysis achieved in this study. Hence, we neglect the heterogeneity of U isotope composition and apply the constant value of 137.88 (*71*). Therefore, ^{206}Pb/^{238}U values were calculated based on the assumed ^{238}U/^{235}U value.

The LA-MC-ICP-MS operational conditions were optimized by the continuous ablation of NIST-SRM612 glass in order to maximize the signal intensity of ^{208}Pb. After the optimization, oxide production rate (^{232}Th^{16}O^{+}/^{232}Th^{+}) was < 0.3%. With an ablation spot size of 35 μm and a repetition rate of 2 Hz, typical signal intensities obtained during ablation of NIST-SRM612 were 6.2×10^4 cps for ^{206}Pb. Typical gas blank levels were 1500 cps for ^{202}Hg, and 30 cps for ^{206}Pb.

Elemental fractionation and instrumental mass bias on ^{206}Pb/^{238}U were corrected using the isotope ratios of the 91500 zircon reference material (*72*) without a correction for common Pb, yielding a reference value of 0.17928 ± 0.00018 (2σ) (*64*). Elemental fractionation for Th/U is calibrated by analyzing radiogenic ^{208}Pb/^{206}Pb on a concordant 91500 zircon reference material with known age (e.g., *73*). Mass bias on ^{207}Pb/^{206}Pb and ^{208}Pb/^{206}Pb were normalized to those of NIST-SRM612 standard glass; 0.90726 and 2.164, respectively (*74*). External reproducibilities of the ^{206}Pb/^{238}U, ^{207}Pb/^{207}Pb, ^{208}Pb/^{206}Pb ratios were determined by repeated analysis of the 91500 zircon and NIST-SRM612. In all analytical sessions involving unknown samples, U–Pb isotope data for Plešovice (337.13 ± 0.37 Ma [*75*]) and OD-3 (33.0 ± 0.1 Ma by SIMS and LA-ICP-MS [*76*]; 32.853 ± 0.016 Ma by ID-TIMS [*77*]) zircons were acquired for use as secondary reference materials.

When U–Pb dating is applied to young zircons, a correction for the initial disequilibria effect associated with intermediate nuclides in the ^{238}U and ^{235}U decay series must be employed (*78–81*). In addition, common Pb correction is also important for Quaternary zircon. In this study, all U–Pb age calculations and error propagation were based on the modified ^{207}Pb method proposed by Sakata (*82*), and actual calculation of ages and errors was conducted by a Microsoft Excel spread sheet provided by that study.

In the modified ^{207}Pb method, Th/U and Pa/U partitioning factors in zircon-melt system and ^{207}Pb/^{206}Pb of common Pb are required. Elemental partitioning factors of Th/U and Pa/U are defined as follows:

$$f_{Th/U} = \frac{(Th/U)_{Zircon}}{(Th/U)_{Melt}} \quad (1)$$

$$f_{Pa/U} = \frac{(Pa/U)_{Zircon}}{(Pa/U)_{Melt}} \quad (2).$$

We determined concentration of Th and U of zircon, grain-by-grain, simultaneously with U–Pb isotope composition using the same LA-MC-ICP-MS instrument. The Th/U in melt is estimated from measuring Th/U in melt inclusion in plagioclase separated from same samples. Melt inclusion measurement is conducted using an Agilent 8800 single-collector triple quadrupole ICP-MS (Agilent Tech., Santa Clara, USA) coupled to a NWR-213 laser-ablation system (ESI, Portland, US), that utilizes a 213 nm Nd:YAG laser. The laser was operated with fluence of 11.0 to 11.4 Jcm^{-2}, repetition rate of 5 Hz, and laser spot size diameter of 4 μm. Ablation duration is 4

s. As primary calibration standard, NIST-SRM610 (Th/U = 0.9858 [*83*]) was used. The resulting U-Th plots of zircons from the BP-LMTCL-1, BP-GB-BC-P1 and Pb-T8 samples treated in this study show a nearly-linear correlation (Fig. S4), and representative values of zircon Th/U are determined to be 0.741 ± 0.032 (1σ, n = 75, MSWD = 50) for BP-LMTCL-1, 0.683 ± 0.040 (1σ, n = 47, MSWD = 4.2) for BP-GB-BC-P1 and 0.908 ± 0.017 (1σ, n = 25, MSWD = 1.4) for Pb-T8. From the measurement of melt inclusions, 13, 15 and 13 Th/U values were obtained from BP-LMTCL-1, BP-GB-BC-P1 and Pb-T8, respectively. The resulting ratios were near-homogeneously distributed, and we calculated weighted average of these values (Fig. S5): 3.82 ± 0.22 (1σ, n = 13, MSWD = 2.2) for BP-LMTCL-1, 3.69 ± 0.26 (1σ, n = 15, MSWD = 3.2) for BP-GB-BC-P1 and 2.59 ± 0.11 (1σ, n = 13, MSWD = 1.7) for Pb-T8. Consequently, the Th/U fractionation factor for disequilibrium correction is determined from Eq. 1: $f_{Th/U}$ = 0.194 ± 0.014 (1σ) for BP-LMTCL-1, $f_{Th/U}$ = 0.185 ± 0.017 (1σ) for BP-GB-BC-P1 and $f_{Th/U}$ = 0.351 ± 0.016 (1σ) for Pb-T8. The other values used for the modified ^{207}Pb method are given in footnote in Table S5, including compiled value (from *64, 67, 84*) of $f_{Pa/U}$ = 3.36 ± 0.20 (1σ, MSWD = 0.77, n = 5). Isotopic composition of common Pb is estimated assuming the terrestrial Pb isotope evolution in continental crust at 0.9 Ma by a two-stage model (^{207}Pb/^{206}Pb = 0.8357) (*85*).

Instrumentation, operational settings, and data reduction procedures are summarized in Tables S3 and S4. Results of isotopic analysis of melt inclusions are shown in Fig. S5. The U–Pb isotopic and calculated age data on zircon grains analyzed in this study are listed in Table S5. All weighted mean values and MSWD values were calculated using Isoplot 4.15 (*86*).

As noted above, the closure temperature of zircon U–Pb choronometry is much higher than that of zircon fission-track choronometry (*48, 49*); the former should provide the time of zircon crystallization which commonly occurs before eruption (*87*), and the latter, the volcanic eruption age. When we deal with young samples as treated here, it is necessary to consider the period of zircon crystallization that may extend for over hundreds of thousand years (> 140 kyr) in a magma reservoir (*63, 67*). Thus, the combination of the two chronometries will be informative and the comparison of the dating results from the two approaches is important (see Fig. 3).

Fig. S1. Sampling sites for dating. See next page for figure caption.

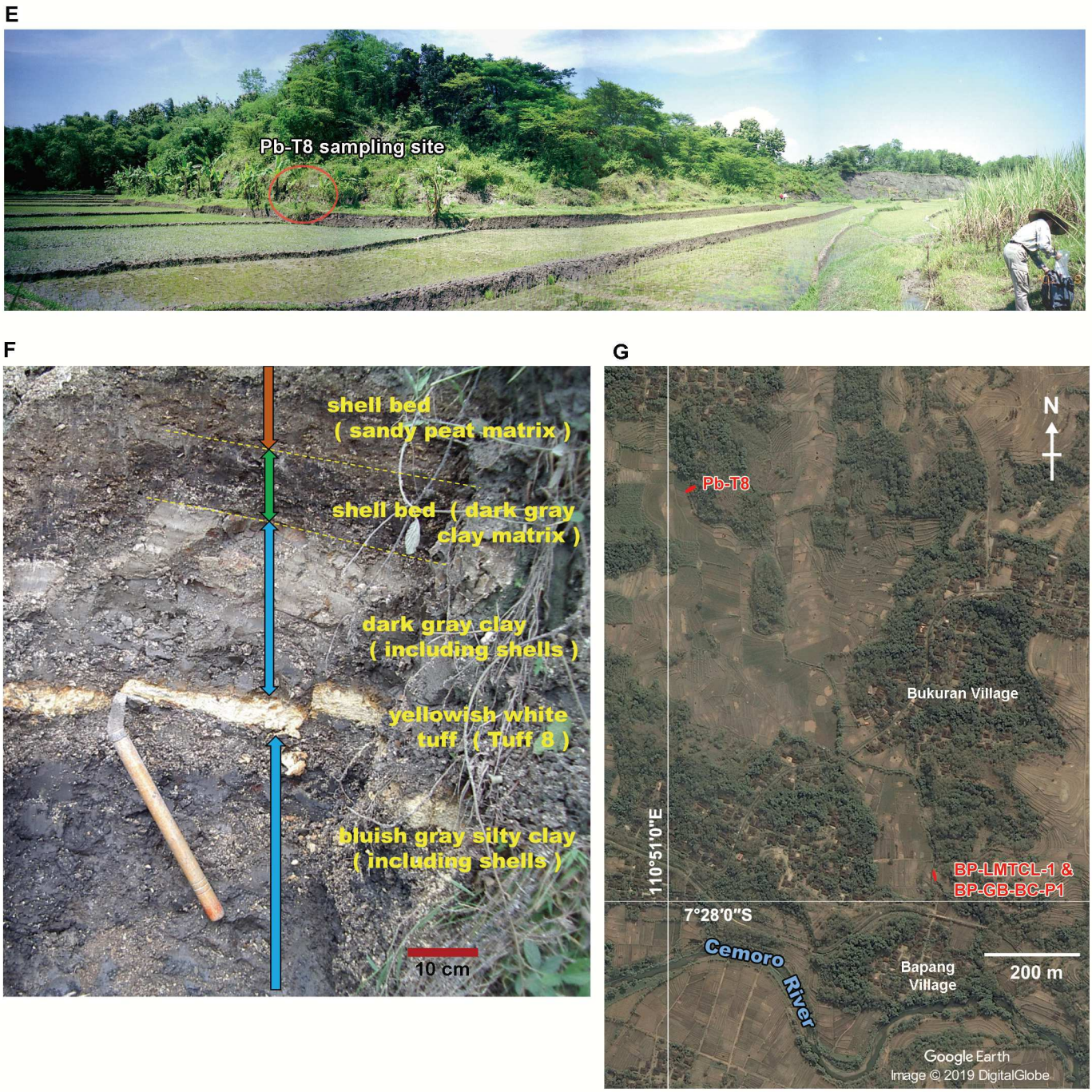

Fig. S1. Sampling sites for dating. (A) Southwest view of the basal part of section S48 (Fig. 1B). The red circle indicates where BP-LMTCL-1 was sampled. BP-GB-BC-P1 was sampled nearby the stream bed below the red arrow marker. (B) A block sample of tuffaceous sand (BP-LMTCL-1) lies to the right of the plastic T-type tag (9.3 cm long and 5.5 cm wide). (C) Close up of cross-stratification within the tuffaceous sand. (D) Pumice sample BP-GB-BC-P1 was taken from the bottom part of the bluish gray clay layer (Fig. 2). (E) Location of the Pb-T8 sampling site, viewed from the southwest. (F) Pb-T8 was sampled from Tuff 8 of the Sangiran Formation (Fig. 1C; Fig. 2). (G) Map of the Bapang and Bukuran districts.

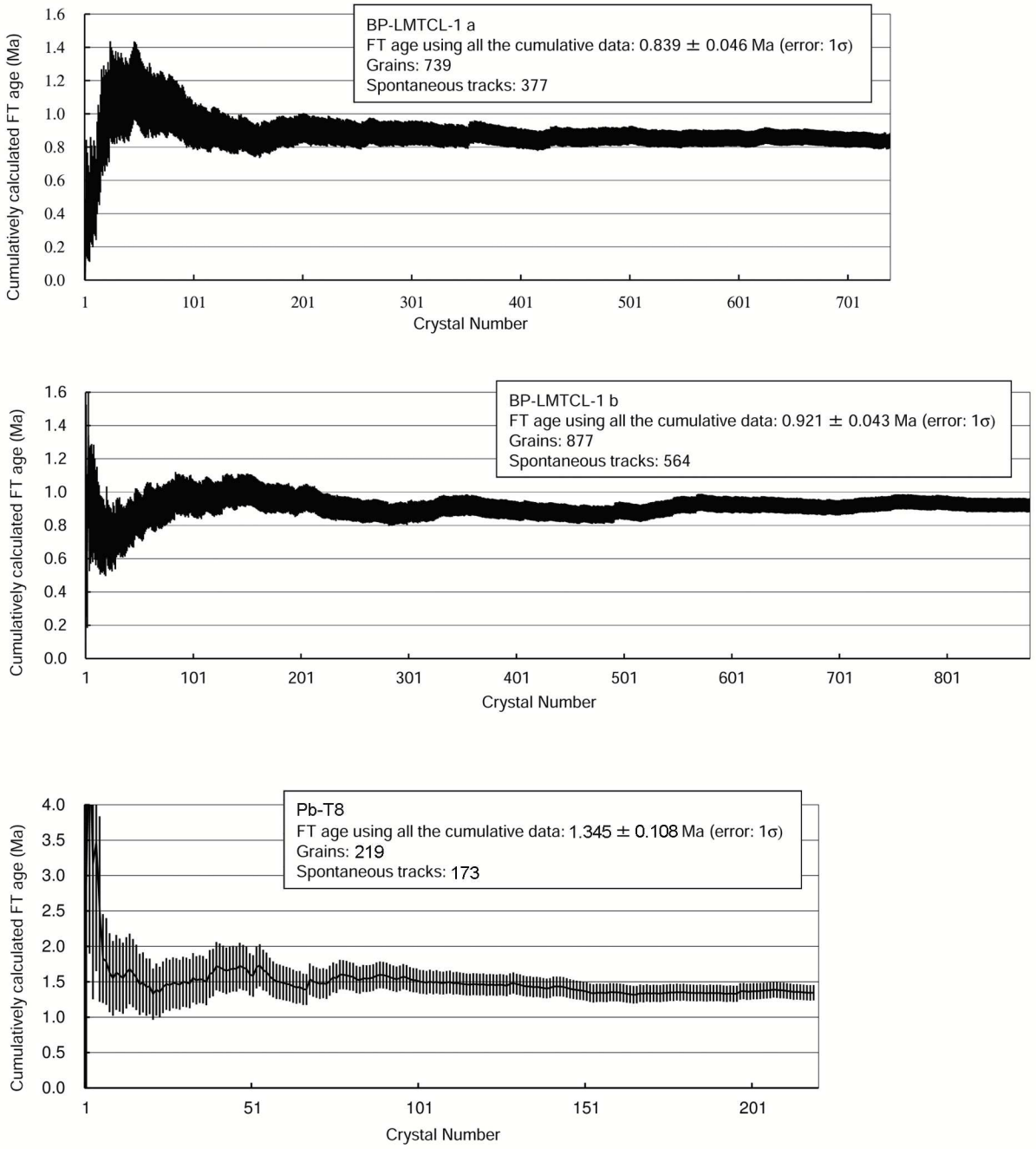

Fig. S2. Zircon fission-track ages of BP-LMTCL-1a, BP-LMTCL-1b and Pb-T8 (see Table S1). The ordinate shows the age (68.2% confidence interval) calculated using all of the grain data up until the crystal number on the abscissa.

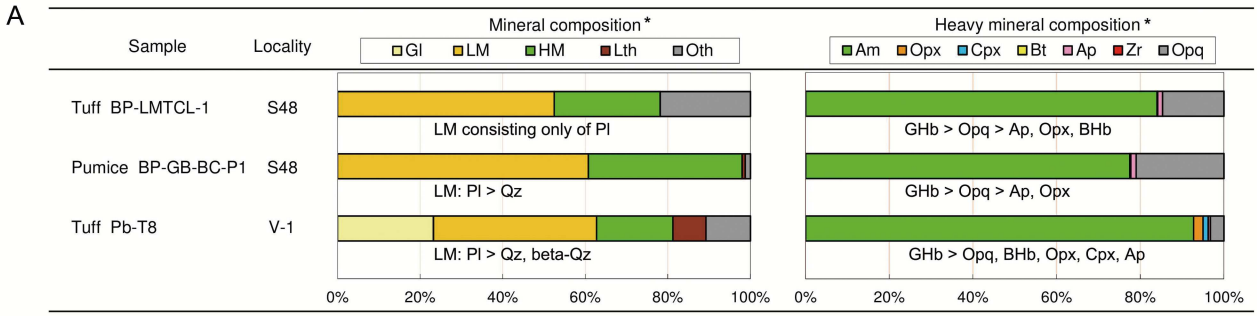

* Average of three runs for BP-LMTCL-1, and of two runs for BP-GB-BC-P1 and Pb-T8; each run is based on counts of 200 grains.
Abbreviations: Gl, volcanic glass; LM, light minerals; HM, heavy minerals; Lth, lithic fragments; Oth, others; Pl, plagioclase; Qz, quartz; Am, amphibole; Opx, orthopyroxene; Cpx, clinopyroxene; Bt, biotite; Ap, apatite; Zr, zircon; Opq, opaque minerals; BHb, brown hornblende; GHb, green hornblende.

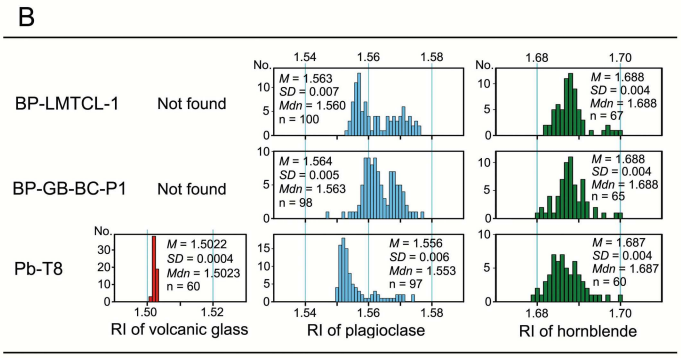

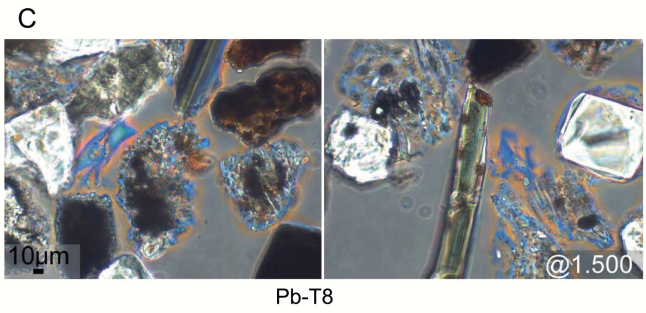

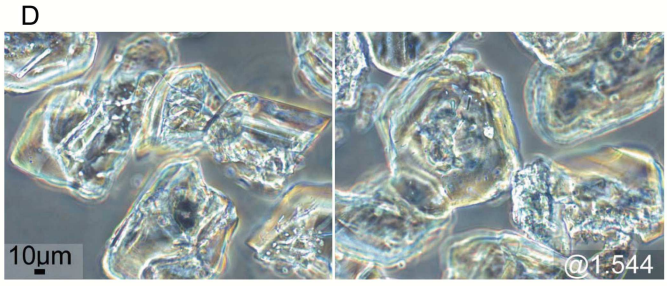

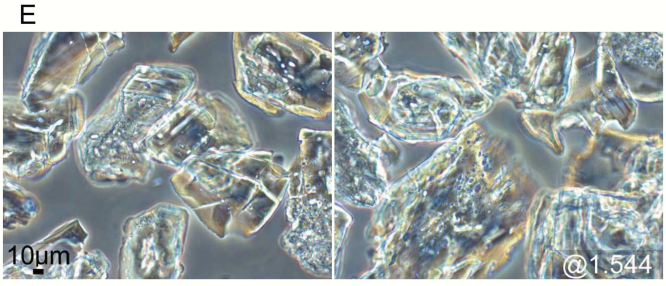

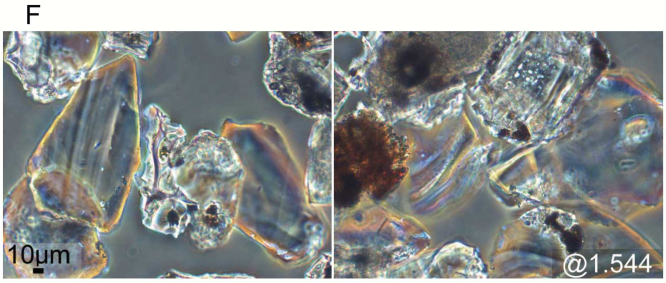

Fig. S3. Tephra analyses of dated samples. (A) Mineral compositions. (B) Refractive index (RI) histograms. (C) Photomicrograph (two panels for Pb-T8) showing volcanic glass shards with immersion oil (RI=1.500) captured using a RIMS analyzer (*33*). Scale bar is common to both panels.
(D, E, F) Photomicrographs (two panels for each sample) showing plagioclase crystals with immersion oil (RI=1.544) captured using a RIMS analyzer (*33*). Scale bar is common to both panels. (G, H, I) Photomicrographs of hornblende crystals (dry) before refractive index measurement.

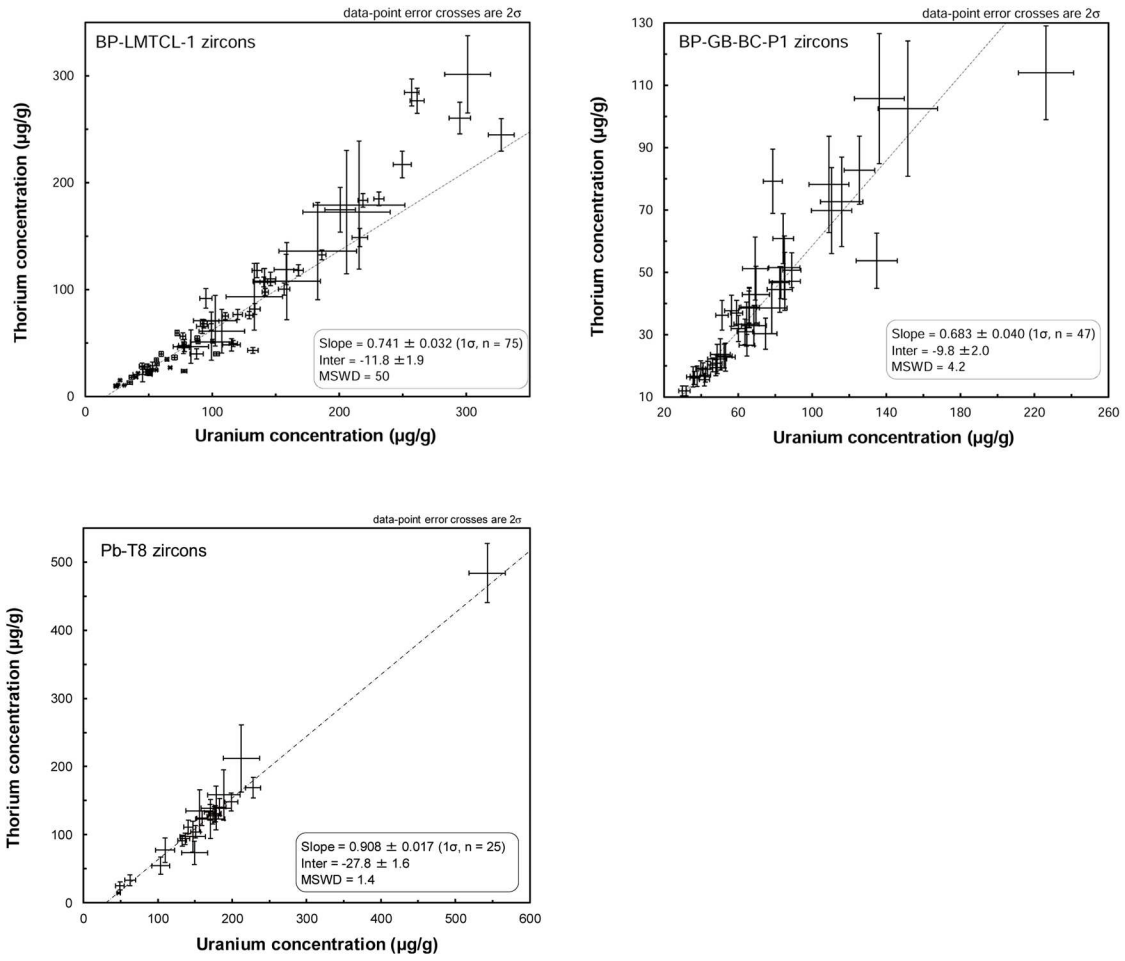

Fig. S4. Concentrations of Th and U in zircon crystals separated from BP-LMTCL-1 (Top left), BP-GB-BC-P1 (Top right) and Pb-T8 (Bottom).

Th and U isotopic analysis of melt inclusions.

Sample name	^{232}Th counts	^{238}U counts	^{232}Th/^{238}U*	1σ†
Melt inclusions hosted in plagioclase separated from BP-LMTCL-1				
BP-LMTCL-1 no.m15	107	29	6.0	1.3
BP-LMTCL-1 no.m20	122	42	4.2	0.8
BP-LMTCL-1 no.m28	163	60	3.9	0.6
BP-LMTCL-1 no.m32	218	66	4.7	0.7
BP-LMTCL-1 no.m38	536	210	3.5	0.3
BP-LMTCL-1 no.m39	153	53	3.9	0.6
BP-LMTCL-1 no.m63	226	70	4.9	0.7
BP-LMTCL-1 no.m64	309	141	3.2	0.3
BP-LMTCL-1 no.m65	150	75	3.1	0.4
BP-LMTCL-1 no.m66	253	78	5.1	0.7
BP-LMTCL-1 no.m73	134	48	4.6	0.8
BP-LMTCL-1 no.m75	439	128	5.0	0.5
BP-LMTCL-1 no.m81	307	133	3.5	0.4
		Wtd. mean	**3.82**	**0.22**
		MSWD	**2.2**	
		n	**13**	
Melt inclusions hosted in plagioclase separated from BP-GB-BC-P1				
BP-GB-BC-P1 no.m02	199	83	3.6	0.5
BP-GB-BC-P1 no.m5	277	105	3.9	0.4
BP-GB-BC-P1 no.m7	129	31	6.5	1.3
BP-GB-BC-P1 no.m10	379	118	4.7	0.5
BP-GB-BC-P1 no.m11	282	86	4.9	0.6
BP-GB-BC-P1 no.m14	161	49	5.4	0.9
BP-GB-BC-P1 no.m16	196	88	3.3	0.4
BP-GB-BC-P1 no.m21	146	57	3.9	0.6
BP-GB-BC-P1 no.m25	226	130	2.6	0.3
BP-GB-BC-P1 no.m26	173	76	3.5	0.5
BP-GB-BC-P1 no.m32	162	71	3.4	0.5
BP-GB-BC-P1 no.m36	168	55	4.6	0.7
BP-GB-BC-P1 no.m48	108	34	4.8	0.9
BP-GB-BC-P1 no.m59	218	76	4.3	0.6
BP-GB-BC-P1 no.m60	158	37	6.9	1.3
		Wtd. mean	**3.69**	**0.26**
		MSWD	**3.2**	
		n	**15**	
Melt inclusions hosted in plagioclase separated from Pb-T8				
0203-Pb-T8 no.m1	269	106	2.1	0.2
0203-Pb-T8 no.m2	225	80	2.3	0.3
0203-Pb-T8 no.m3	235	81	2.4	0.3
0203-Pb-T8 no.m4	296	102	2.4	0.3
0203-Pb-T8 no.m7	221	74	2.5	0.3
0203-Pb-T8 no.m12	728	244	2.6	0.2
0203-Pb-T8 no.m17	125	43	2.5	0.5
0203-Pb-T8 no.m26-2	434	164	2.5	0.2
0203-Pb-T8 no.m32	228	91	2.4	0.3
0203-Pb-T8 no.m33	335	95	3.3	0.4
0203-Pb-T8 no.m38	165	46	3.5	0.6
0203-Pb-T8 no.m41	788	247	3.1	0.2
0203-Pb-T8 no.m43	444	146	3.0	0.3
		Wtd. mean	**2.59**	**0.11**
		MSWD	**1.7**	
		n	**13**	

* Th/U elemental fractionation factor is linearly interpolated by repeated analysis of NIST-SRM610 (Th = 450.6 μg/g, U = 457.1 [*83*]).

† Analytical error is consisted of internal precision estimated from counting statistics of Th and U, and reproducibility of repeated analysis of calibration standard.

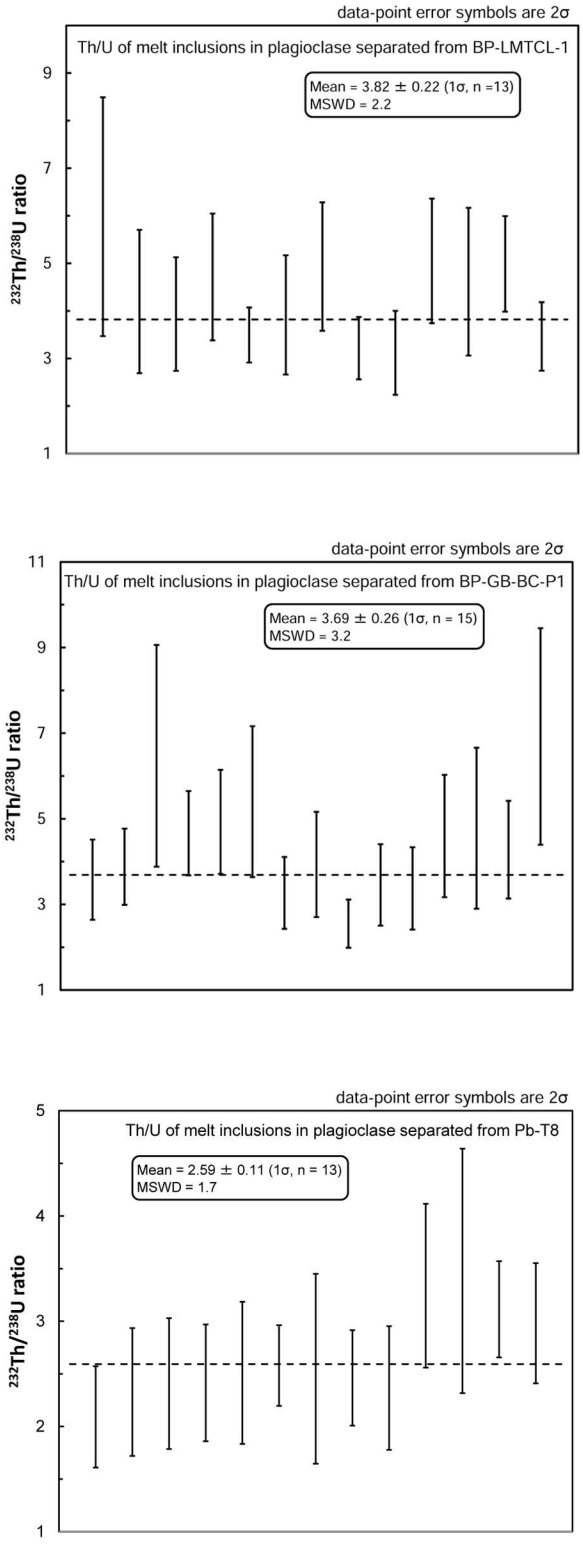

Fig. S5. Th and U analysis of melt inclusions in plagioclase, separated from BP-LMTCL-1 (Top), BP-GB-BC-P1 (Middle) and Pb-T8 (Bottom).

Table S1. Results of zircon fission-track dating of tephra samples (BP-LMTCL-1 and Pb-T8) from the Sangiran area, and the Fish Canyon Tuff standard.

Zircon Sample ID	Method*	Detector†	No. of grains	Spontaneous		Induced		Dosimetry‡§		Pr(χ^2)¶	U-content	Age ± 1σ #, **, ††,‡‡, §§
				ρ_s (cm^{-2})	N_s	ρ_i (cm^{-2})	N_i	ρ_d (cm^{-2})	N_d	(%)	(ppm)	(Ma)
BP-LMTCL-1 a	ED2	DAP	739	2.38 ×10 ^{4}	*377*	9.150 ×10 ^{5}	*14502*	9.063 ×10 ^{4}	*4640*	71	80	0.839 ± 0.046
BP-LMTCL-1 b	ED2	DAP	877	2.70 ×10 ^{4}	*564*	8.710 ×10 ^{5}	*18221*	8.357 ×10 ^{4}	*4279*	62	90	0.921 ± 0.043
										Weighted mean:		**0.884 ± 0.031**
Pb-T8	ED2	DAP	219	8.94 ×10 ^{4}	*173*	2.310 ×10 ^{5}	*4469*	9.763 ×10 ^{4}	*2499*	99	190	1.345 ± 0.108
Fish Canyon Tuff a	ED2	DAP	30	3.535 ×10 ^{6}	*3012*	3.912 ×10 ^{6}	*3333*	9.186 ×10 ^{4}	*4703*	3	350	29.49 ± 0.89
Fish Canyon Tuff b	ED2	DAP	30	3.694 ×10 ^{6}	*2865*	3.763 ×10 ^{6}	*2918*	8.407 ×10 ^{4}	*4304*	14	370	29.32 ± 0.92

* External detector method that applies to external natural surfaces of zircon (ED2)

† Detector: diallyl phthalate (DAP) plastic detector

‡ Thermal neutron dosimetry: NIST-SRM612 glass

§ Irradiation facility: pneumatic tube of JRR-4 reacor unit of Japan Atomic Energy Agency (JAEA)

¶ Pr(χ^2): the probability of obtaining the χ^2-value for n degrees of freedom (where n = number of grains – 1) (*88*)

Age equation: $t = (1/\lambda_D) \ln [1 + \lambda_D \zeta (g\rho_s/\rho_i) \rho_d]$ for zeta age calibration (g, geometry factor of 1 for ED2; r, track density)

** Error: $\sigma_t = t \times[1/\Sigma N_s+1/\Sigma N_i+1/\Sigma N_d+(\sigma_\zeta/\zeta)^2]^{1/2}$ (N, the total number of fission tracks counted)

†† Constants: the total decay constant of ^{238}U: $\lambda_D = 1.55125\times10^{-10}$ yr^{-1}

‡‡ ζ-calibration factor for T. Danhara: $\zeta_{ED2} = 356 \pm 3$, recalibrated from Danhara *et al.* (*40*), based on U-Pb ages as reference (see ref *24*)

§§ Ages from the two fission-track dating experiments (on BP-LMTCL-1a and BP-LMTCL-1b subsamples) agree within 2 sigma statistical errors and have no significant difference (P=0.19, z-test, two-side), yielding a weighted mean age of 0.884 ± 0.031 Ma.

Table S2. U-Pb dating of the Buluk Member Tuff by the laser-ablation inductively-coupled plasma mass spectrometry.

U-Pb isotopic and age data on zircon grains* from the Buluk Member Tuff (IUGS age standard)

Sample name	Isotopic ratio				Age (Ma)		Concentration (μg/g) and ratio†		
(Analysed spot ID)	$^{206}Pb/^{238}U$	2σ	$^{207}Pb/^{206}Pb$	2σ	^{238}U-^{206}Pb	2σ	U	Th	Th/U
FTBM4I13 no.2(3)	0.002432 ±	0.000104	0.0542 ±	0.0015	15.7 ±	0.7	118	79	0.67
FTBM4I13 no.3(3)	0.002562 ±	0.000131	0.0553 ±	0.0015	16.5 ±	0.8	66	34	0.52
FTBM4I13 no.4(3)	0.002617 ±	0.000115	0.0505 ±	0.0014	16.8 ±	0.7	99	60	0.60
FTBM4I13 no.5(2)	0.002569 ±	0.000115	0.0456 ±	0.0013	16.5 ±	0.7	96	57	0.60
FTBM4I13 no.8	0.002609 ±	0.000106	0.0523 ±	0.0015	16.8 ±	0.7	128	106	0.82
FTBM4I13 no.9	0.002587 ±	0.000116	0.0412 ±	0.0011	16.7 ±	0.7	94	51	0.55
FTBM4I13 no.10	0.002531 ±	0.000141	0.0367 ±	0.0010	16.3 ±	0.9	52	28	0.53
FTBM4I13 no.11	0.002564 ±	0.000110	0.0509 ±	0.0014	16.5 ±	0.7	109	73	0.68
FTBM4I13 no.12	0.002459 ±	0.000110	0.0483 ±	0.0013	15.8 ±	0.7	101	63	0.62
FTBM4I13 no.13	0.002351 ±	0.000124	0.0532 ±	0.0015	15.1 ±	0.8	65	38	0.59
FTBM4I13 no.14	0.002310 ±	0.000087	0.0464 ±	0.0013	14.9 ±	0.6	194	180	0.93
FTBM4I13 no.15	0.002453 ±	0.000126	0.0421 ±	0.0012	15.8 ±	0.8	67	39	0.58
FTBM4I13 no.16	0.002576 ±	0.000143	0.0467 ±	0.0013	16.6 ±	0.9	52	27	0.51
FTBM4I13 no.17	0.002557 ±	0.000105	0.0528 ±	0.0015	16.5 ±	0.7	127	103	0.81
FTBM4I13 no.19	0.002468 ±	0.000105	0.0445 ±	0.0012	15.9 ±	0.7	117	81	0.69
FTBM4I13 no.20	0.002450 ±	0.000101	0.0467 ±	0.0013	15.8 ±	0.7	130	102	0.79
			Mean ± 2σ (n=16)		**16.1**	**± 0.3**			

Instrumentation and operational settings

Laser ablation	
Model	New Wave Research NWR193
Laser type (Wave length)	Excimer ArF (193nm)
Energy density	2.6 J/cm^2
Crater size	35 mm
Sampling mode	single spot ablation with 3 pre-ablation shots
Repetition rate	10 Hz
Carrier gas	He
Ablation duration	20 s
ICP mass spectrometry	
Model	Nu Instruments AttoM
ICP-MS type	Magnetic sector field
Forward power	1300 W
Make-up gas	Ar
Ar gas flow rate	0.93 L min^{-1}
He gas flow rate	0.65 L min^{-1}
Scanning mode	Deflector jump
Monitor isotopes	^{202}Hg, ^{204}Pb, ^{206}Pb, ^{207}Pb, ^{208}Pb, ^{232}Th, ^{238}U
Data acquisition protocol	Integration of ion counts per ablation (Batch)
Dwell time and number of sweep	U-Pb dating: 1 ms of dwell time for all isotopes monitored and 1000 sweeps (total integration time was 8 s)
Blank correction	Gas blank
$^{232}Th^{16}O$ formation rate	< 1%
Primary standard	91500[‡]
Secondary standard	Plešovice[§], OD3[¶#]

Accompanying analysis on the secondary standards (Plešovice of 337.13 Ma and OD-3 of 33.0 Ma) for measurement quality control yielded ^{238}U-^{206}Pb ages of 337.4 ± 2.5 (2σ) Ma (n=16) and 33.0 ± 0.4 (2σ) Ma (n=18), respectively. For Plešovice and OD-3, see ref *24*.

* Passed the test for concordance of U-Pb systematics

† Based on a measured value of 74 ppm for 91500 primary standard used and a reported Th/U value of 0.3444 (*72*)

‡ Wiedenbeck *et al.* (*72*)

§ Sláma *et al.* (*75*)

¶ Iwano *et al.* (*76*)

Lukács *et al.* (*77*)

Table S3. Instrumentation and operational settings for U-Pb dating and melt inclusion measurement.

U-Pb daring		Melt inclusion measurement	
Laser ablation system		**Laser ablation system**	
Instrument	NWR193 excimer laser (ESI, Portland, USA)	Instrument	NWR-213 Nd:YAG laser (ESI, Portland, USA)
Cell type	Two volume cell	Cell type	Two volume cell 2
Laser wave length	193 nm	Laser wave length	213 nm
Pulse duration	<5 ns	Pulse duration	<5 ns
Fluence	2.1 J/cm^2	Fluence	11.0-11.4 J/cm^2
Repetition rate	2 Hz	Repetition rate	5 Hz
Ablation pit size	35 μm	Ablation pit size	4 μm
Sampling mode	Single hole drilling	Sampling mode	Single hole drilling
Pre-cleaning	1 shot with 50 μm	Pre-cleaning	1 shot with 15 μm
Carrier gas	He gas and Ar make-up gas combined outside ablation cell	Carrier gas	He gas and Ar make-up gas combined outside ablation cell
He gas flow rate	0.50 l/min	He gas flow rate	0.60 l/min
Ar make-up gas flow rate	0.84 l/min	Ar make-up gas flow rate	1.22 l/min
Ablation duration	25 s	Ablation duration	4 s
Signal smoothing device	Enabled (*65*)	Signal smoothing device	Not used
ICP Mass Spectrometer		**ICP Mass Spectrometer**	
Instrument	Nu PlasmaII HR-MC-ICP-MS (Nu Instruments, Wrexham, U.K.)	Instrument	Agilent 8800 (Agilent Tech., Santa Clara, USA)
RF power	1300 W	RF power	1500 W
Data reduction	Integration of total ion counts per single ablation. Signals obtaind from first few seconds were not used for data reduction, and next signals obtained from 18 seconds were integrated for further calculations. Intensity of ^{238}U is calculated assuming ^{238}U/^{235}U = 137.88 (*71*).	Data reduction	Integration of total ion counts per single ablation.
Detection mode	Multiple collector mode	Detection mode	Pulse counting mode
Detector	Five full size secondary electron multipliers (IC0, IC1, IC3, IC4 and IC5), one daly collector (D2), and one faraday cup (H9) were used	Detector	Signle electron multiplier
Dead time	ICO: 15.8 ns, IC1: 15.0 ns, IC3: 14.7 ns, IC4: 18.9 ns, IC5: 20.0 ns, D2: 8.6 ns	Dead time	15 ns
Monitored isotopes	^{202}Hg, ^{204}(Hg + Pb), ^{206}Pb, ^{207}Pb, ^{208}Pb, ^{232}Th, ^{235}U	Monitored isotopes	^{232}Th, ^{238}U
Integration time per peak	18 s	Integration time per peak	5 s
Total integration time per reading	0.4 s	Dwell time	100 ms for ^{232}Th and ^{238}U
Formation rate of ^{232}Th^{16}O	<0.3%	Formation rate of ^{232}Th^{16}O	<3%
Data processing		**Data processing**	
Gas blank	Gas blank counts were obtained for 18 s before each ablation pit.	Gas blank	Gas blank counts were obtained for 25 s before each ablation pit.
Calibration strategy	91500 zircon was used in correction for Pb/U fractionation and difference of detector's gain in all measurements. NIST SRM612 was used for correction of Pb/Pb mass bias and difference of detector's gain as well. Plešovice (337.13 Ma [*75*]) and OD-3 (32.853 ± 0.016 Ma [*77*]) were used as secondary standards for quality control	Calibration strategy /Normalization values	Th/U elemental fractionation factor is linearly interpolated by repeated analysis of NIST SRM610 (Th = 450.6 μg/g, U = 457.1 [*83*]).
Normalization values	^{206}Pb/^{238}U = 0.1793, U concentration = 81.2 μg/g, Th concentration = 28.6 μg/g (91500 zircon [*72*]), ^{207}Pb/^{206}Pb = 0.90726, ^{206}Pb/^{204}Pb = 17.093, ^{207}Pb/^{204}Pb = 15.509, ^{208}Pb/^{204}Pb = 36.999 for NIST-SRM612 (*74*).	Uncertainties	Analytical error is consisted of internal precision estimated from counting statistics of Th and U, and reproducibility of repeated analysis of calibration standard.
Disequilibrium/common-Pb correction	Corrected ages are calculated considering both the effect of initial disequilibrium and the common Pb contribution (see text for explanation). Values used for the disequilibrium/common-Pb correction are given in footnote in Table S5.		
Uncertainties	Uncertainties for ages and isotope ratios are quoted at 2 sd absolute, propagation is by quadratic addition. Reproducibilities of primary standard, counting statistics of measured isotopes, errors on fractionation factor (*f*), and uncertainties of reference values of 91500 zircon are propagated.		
Quality control/validation	For Plešovice and OD-3 (secondary reference materials), see Table S5.		

Table S4. Collector configurations used on the Nu Plasma II for the U-Pb isotope analysis.

Detector*	IC5	H10	H9	H8	H7	H6	H5	H4	H3	H2	H1	Ax	L1	L2	L3	L4	L5	IC0	IC1	D2	IC3	IC4
Amu	235		232															208	207	206	204	202
Isotopes	U		Th															Pb	Pb	Pb	Pb, Hg	Hg

Note the gaps in the collector assembly between H10 and H9, H9 and H8, D2 and IC3, and IC3 and IC4.

* H10 to H1, Ax, and L1 to L5 are faraday cups, IC0 to IC5 are secondary electron multipliers, and D2 is daly collector.

Table S5. U-Pb isotopic and calculated age data on zircon grains.

Sample name	Isotopic ratio				^{238}U-^{206}Pb age without correction (Ma)		Disequilibrium-corrected ^{238}U-^{206}Pb age (Ma)		Disequilibrium & common Pb-corrected U-Pb age (Ma)*		Elemental concentration (μg/g) and ratio					
	$^{206}Pb/^{238}U$	1σ	$^{207}Pb/^{206}Pb$	1σ		1σ		1σ		1σ	U	1σ	Th	1σ	Th/U	1σ
Zircons separated from BP-LMTCL-1																
BP-LMTCL-1 no.b004	0.000171	0.000006	0.098	0.014	1.104	0.041	1.192	0.045	1.130	0.042	23.9	0.6	10.0	0.5	0.418	0.003
BP-LMTCL-1 no.b005	0.000139	0.000005	0.110	0.013	0.894	0.031	0.982	0.034	0.921	0.032	50.2	1.3	21.7	1.1	0.433	0.003
BP-LMTCL-1 no.b006	0.000161	0.000005	0.175	0.016	1.036	0.033	1.124	0.036	0.967	0.034	36.4	0.9	18.0	0.9	0.496	0.004
BP-LMTCL-1 no.b009	0.000142	0.000003	0.078	0.007	0.918	0.020	1.006	0.023	0.980	0.020	92.2	2.3	65.6	3.3	0.712	0.006
BP-LMTCL-1 no.b012	0.000136	0.000005	0.178	0.018	0.874	0.031	0.962	0.034	0.827	0.032	48.6	1.2	27.7	1.4	0.569	0.004
BP-LMTCL-1 no.b014	0.000140	0.000004	0.036	0.006	0.905	0.028	0.993	0.030	0.993	0.028	44.8	1.1	28.4	1.4	0.634	0.005
BP-LMTCL-1 no.b015	0.000138	0.000003	0.088	0.007	0.889	0.019	0.976	0.022	0.941	0.020	94.9	2.4	91.8	4.6	0.967	0.008
BP-LMTCL-1 no.b017	0.000161	0.000004	0.099	0.010	1.036	0.028	1.123	0.031	1.066	0.029	48.9	0.7	23.3	0.7	0.477	0.004
BP-LMTCL-1 no.b018	0.000145	0.000004	0.111	0.010	0.934	0.025	1.021	0.028	0.957	0.025	56.0	0.8	34.1	1.0	0.609	0.005
BP-LMTCL-1 no.b021	0.000147	0.000006	0.213	0.022	0.948	0.037	1.035	0.039	0.846	0.038	25.7	0.4	11.1	0.3	0.430	0.003
BP-LMTCL-1 no.b023	0.000140	0.000004	0.129	0.011	0.903	0.024	0.991	0.027	0.908	0.025	56.5	0.8	30.7	0.9	0.543	0.004
BP-LMTCL-1 no.b025	0.000139	0.000002	0.055	0.003	0.894	0.011	0.982	0.014	0.982	0.011	294.9	4.2	260.5	7.4	0.883	0.007
BP-LMTCL-1 no.b026	0.000128	0.000004	0.069	0.010	0.827	0.027	0.914	0.030	0.902	0.028	40.0	0.6	18.2	0.5	0.456	0.004
BP-LMTCL-1 no.b030	0.000130	0.000002	0.062	0.005	0.839	0.015	0.927	0.018	0.922	0.016	135.2	1.9	117.9	3.4	0.872	0.007
BP-LMTCL-1 no.b031	0.000164	0.000006	0.072	0.011	1.057	0.038	1.144	0.041	1.121	0.038	27.3	0.4	15.2	0.4	0.558	0.004
BP-LMTCL-1 no.b034	0.000139	0.000003	0.077	0.007	0.898	0.021	0.986	0.024	0.962	0.021	76.8	1.1	56.3	1.6	0.733	0.006
BP-LMTCL-1 no.b035	0.000184	0.000003	0.237	0.011	1.185	0.022	1.273	0.025	0.997	0.023	93.3	1.3	68.0	1.9	0.729	0.006
BP-LMTCL-1 no.b036	0.000142	0.000003	0.074	0.007	0.914	0.022	1.002	0.025	0.981	0.022	72.2	0.8	59.4	1.3	0.822	0.005
BP-LMTCL-1 no.b038	0.000138	0.000002	0.067	0.004	0.892	0.012	0.980	0.015	0.968	0.012	261.3	2.8	276.7	5.9	1.059	0.006
BP-LMTCL-1 no.b044	0.000147	0.000004	0.114	0.011	0.946	0.026	1.034	0.029	0.964	0.027	52.2	0.6	25.0	0.5	0.479	0.003
BP-LMTCL-1 no.b045	0.000150	0.000003	0.088	0.008	0.967	0.022	1.054	0.025	1.014	0.022	77.8	0.8	49.0	1.0	0.630	0.004
BP-LMTCL-1 no.b048	0.000146	0.000003	0.059	0.006	0.939	0.020	1.027	0.023	1.023	0.021	88.2	0.9	54.4	1.2	0.617	0.004
BP-LMTCL-1 no.b049	0.000142	0.000004	0.055	0.007	0.915	0.023	1.003	0.026	1.003	0.023	64.3	0.7	34.8	0.7	0.541	0.003
BP-LMTCL-1 no.b050	0.000146	0.000003	0.035	0.004	0.939	0.018	1.027	0.021	1.027	0.018	110.3	1.2	75.2	1.6	0.682	0.004
BP-LMTCL-1 no.b052	0.000151	0.000005	0.060	0.009	0.972	0.030	1.060	0.032	1.054	0.030	41.5	0.4	21.8	0.5	0.525	0.003
BP-LMTCL-1 no.b053	0.000148	0.000003	0.041	0.004	0.953	0.016	1.041	0.019	1.041	0.017	140.5	1.5	107.2	2.3	0.763	0.005
BP-LMTCL-1 no.b056	0.000130	0.000006	0.104	0.016	0.836	0.037	0.924	0.039	0.874	0.037	24.3	0.7	9.5	0.6	0.392	0.004
BP-LMTCL-1 no.b057	0.000144	0.000002	0.047	0.004	0.927	0.015	1.015	0.018	1.015	0.015	200.7	6.0	174.7	10.5	0.870	0.009
BP-LMTCL-1 no.b059	0.000148	0.000005	0.172	0.017	0.957	0.033	1.045	0.036	0.903	0.034	35.0	1.0	12.9	0.8	0.370	0.004
BP-LMTCL-1 no.b061	0.000151	0.000003	0.089	0.006	0.975	0.019	1.063	0.022	1.021	0.020	115.1	3.4	48.3	2.9	0.420	0.005
BP-LMTCL-1 no.b062	0.000150	0.000003	0.100	0.006	0.967	0.017	1.054	0.020	0.999	0.018	141.2	4.2	107.0	6.4	0.758	0.008
BP-LMTCL-1 no.b063	0.000138	0.000004	0.111	0.011	0.891	0.026	0.979	0.029	0.917	0.027	52.9	1.6	28.8	1.7	0.544	0.006
BP-LMTCL-1 no.b064	0.000154	0.000003	0.104	0.008	0.994	0.022	1.082	0.025	1.020	0.022	87.6	2.6	39.9	2.4	0.455	0.005
BP-LMTCL-1 no.b065	0.000144	0.000002	0.052	0.003	0.929	0.013	1.017	0.015	1.017	0.013	301.1	9.0	301.4	18.1	1.001	0.011
BP-LMTCL-1 no.b067	0.000148	0.000003	0.062	0.006	0.954	0.020	1.042	0.023	1.034	0.021	99.3	3.0	70.6	4.2	0.711	0.008
BP-LMTCL-1 no.b068	0.000132	0.000003	0.079	0.008	0.854	0.021	0.941	0.024	0.917	0.022	77.3	2.3	45.7	2.7	0.591	0.006
BP-LMTCL-1 no.b069	0.000148	0.000003	0.025	0.004	0.952	0.023	1.039	0.025	1.039	0.023	78.1	2.3	47.8	2.9	0.612	0.007
BP-LMTCL-1 no.b070	0.000142	0.000004	0.050	0.008	0.914	0.028	1.001	0.030	1.001	0.028	48.3	1.4	23.0	1.4	0.475	0.005
BP-LMTCL-1 no.b071	0.000143	0.000003	0.051	0.004	0.922	0.016	1.010	0.019	1.010	0.016	158.2	4.7	118.8	7.1	0.751	0.008
BP-LMTCL-1 no.b074	0.000140	0.000002	0.054	0.004	0.905	0.016	0.993	0.019	0.993	0.016	145.9	2.1	110.0	3.1	0.754	0.006
BP-LMTCL-1 no.b075	0.000147	0.000002	0.054	0.004	0.948	0.016	1.035	0.019	1.035	0.016	156.6	2.2	100.5	2.9	0.642	0.005
BP-LMTCL-1 no.b076	0.000141	0.000003	0.086	0.008	0.908	0.021	0.995	0.024	0.960	0.022	77.8	1.1	23.9	0.7	0.307	0.003
BP-LMTCL-1 no.b078	0.000143	0.000003	0.065	0.006	0.919	0.018	1.006	0.021	0.996	0.018	116.5	1.7	49.6	1.4	0.425	0.004
BP-LMTCL-1 no.b080	0.000143	0.000002	0.075	0.004	0.920	0.013	1.008	0.015	0.986	0.013	249.6	3.6	217.0	6.2	0.870	0.007
BP-LMTCL-1 no.b083	0.000161	0.000004	0.075	0.008	1.037	0.026	1.125	0.029	1.099	0.026	59.8	0.9	39.8	1.1	0.666	0.006
BP-LMTCL-1 no.b087	0.000139	0.000002	0.051	0.004	0.897	0.013	0.985	0.016	0.985	0.013	216.2	3.1	148.8	4.2	0.688	0.006
BP-LMTCL-1 no.b098	0.000148	0.000004	0.097	0.010	0.955	0.028	1.043	0.031	0.993	0.028	50.6	0.8	23.2	0.7	0.458	0.004
BP-LMTCL-1 no.b099	0.000140	0.000003	0.057	0.005	0.904	0.018	0.991	0.021	0.991	0.019	120.0	1.9	76.8	2.4	0.640	0.006
BP-LMTCL-1 no.b103	0.000139	0.000003	0.094	0.008	0.897	0.021	0.984	0.023	0.941	0.021	133.5	2.1	81.8	2.6	0.613	0.005
BP-LMTCL-1 no.b105	0.000139	0.000002	0.059	0.003	0.896	0.013	0.984	0.016	0.981	0.013	327.5	5.1	244.8	7.6	0.747	0.006
BP-LMTCL-1 no.b107	0.000136	0.000004	0.047	0.006	0.876	0.023	0.963	0.025	0.963	0.023	70.2	1.1	36.5	1.1	0.520	0.005
BP-LMTCL-1 no.b108	0.000149	0.000003	0.056	0.005	0.962	0.021	1.049	0.024	1.049	0.021	132.0	2.1	43.2	1.3	0.327	0.003
BP-LMTCL-1 no.b109	0.000150	0.000003	0.024	0.004	0.967	0.023	1.055	0.025	1.055	0.023	83.1	6.9	46.7	7.8	0.562	0.011
BP-LMTCL-1 no.b110	0.000149	0.000003	0.029	0.004	0.959	0.020	1.047	0.023	1.047	0.020	107.5	9.0	61.1	10.2	0.568	0.011
BP-LMTCL-1 no.b111	0.000136	0.000003	0.082	0.007	0.878	0.019	0.966	0.022	0.938	0.020	102.3	8.5	70.9	11.8	0.693	0.013
BP-LMTCL-1 no.b112	0.000149	0.000003	0.032	0.004	0.958	0.018	1.045	0.021	1.045	0.018	133.1	11.1	93.4	15.6	0.702	0.014
BP-LMTCL-1 no.b113	0.000137	0.000002	0.081	0.005	0.883	0.015	0.971	0.018	0.944	0.015	183.0	15.3	136.0	22.7	0.743	0.014
BP-LMTCL-1 no.b115	0.000143	0.000003	0.023	0.003	0.920	0.016	1.007	0.019	1.007	0.016	158.6	13.3	107.9	18.0	0.680	0.013
BP-LMTCL-1 no.b116	0.000161	0.000005	0.102	0.011	1.035	0.031	1.123	0.034	1.061	0.032	45.1	3.8	20.7	3.5	0.459	0.009
BP-LMTCL-1 no.b118	0.000142	0.000002	0.062	0.004	0.915	0.014	1.003	0.017	0.996	0.015	215.6	18.0	179.1	29.9	0.831	0.016
BP-LMTCL-1 no.b120	0.000143	0.000002	0.053	0.004	0.920	0.014	1.007	0.017	1.007	0.015	205.7	17.2	172.5	28.8	0.839	0.016
BP-LMTCL-1 no.b123	0.000149	0.000003	0.111	0.008	0.960	0.021	1.048	0.024	0.981	0.021	99.3	8.3	51.0	8.5	0.514	0.010
BP-LMTCL-1 no.b125	0.000143	0.000003	0.065	0.006	0.919	0.020	1.007	0.023	0.996	0.020	100.5	0.9	51.8	0.9	0.515	0.007
BP-LMTCL-1 no.b126	0.000143	0.000003	0.044	0.005	0.919	0.021	1.006	0.024	1.006	0.021	88.8	0.8	51.2	0.9	0.576	0.007
BP-LMTCL-1 no.b127	0.000139	0.000004	0.085	0.010	0.896	0.026	0.984	0.028	0.950	0.026	56.0	0.5	24.8	0.4	0.444	0.006
BP-LMTCL-1 no.b129	0.000141	0.000003	0.067	0.005	0.907	0.017	0.995	0.020	0.982	0.017	141.8	1.2	97.7	1.7	0.689	0.009
BP-LMTCL-1 no.b130	0.000139	0.000004	0.026	0.005	0.898	0.024	0.986	0.026	0.986	0.024	66.8	0.6	27.1	0.5	0.405	0.005
BP-LMTCL-1 no.b131	0.000140	0.000002	0.040	0.003	0.903	0.014	0.990	0.016	0.990	0.014	231.2	2.0	184.9	3.2	0.800	0.010
BP-LMTCL-1 no.b134	0.000148	0.000002	0.060	0.004	0.954	0.014	1.041	0.017	1.036	0.015	218.6	1.9	183.5	3.2	0.839	0.011
BP-LMTCL-1 no.b135	0.000141	0.000002	0.028	0.003	0.906	0.015	0.993	0.018	0.993	0.015	186.3	1.6	132.5	2.3	0.712	0.009
BP-LMTCL-1 no.b139	0.000140	0.000002	0.013	0.002	0.901	0.016	0.989	0.018	0.989	0.016	167.9	1.9	118.1	2.6	0.703	0.006
BP-LMTCL-1 no.b140	0.000144	0.000003	0.062	0.005	0.925	0.018	1.013	0.021	1.005	0.018	129.1	1.4	76.0	1.7	0.589	0.005
BP-LMTCL-1 no.b142	0.000135	0.000002	0.068	0.004	0.870	0.013	0.958	0.016	0.945	0.013	257.0	2.9	284.5	6.3	1.107	0.010
BP-LMTCL-1 no.b148	0.000141	0.000003	0.069	0.006	0.906	0.019	0.994	0.022	0.979	0.020	103.3	1.1	39.9	0.9	0.386	0.003
BP-LMTCL-1 no.b149	0.000135	0.000005	0.073	0.012	0.868	0.034	0.956	0.037	0.938	0.034	30.6	0.3	10.5	0.2	0.343	0.003
			Wtd. mean ± 1σ		**0.922 ± 0.006**		**1.010 ± 0.006**		**0.991 ± 0.005**							
			MSWD		**6.0**		**4.6**		**4.5**							
			n		**75**		**75**		**75**							

* Corrected ages are calculated considering both the effect of initial disequilibrium and the common Pb contribution (see text for explanation). As estimation of Th/U and Pa/U partioning in zircon-melt system, following values are applied: $f_{Th/U}$ = 0.194 ± 0.014 (1σ) for BP-LMTCL-1, $f_{Th/U}$ = 0.185 ± 0.017 (1σ) for BP-GB-BC-P1, and $f_{Th/U}$ = 0.351 ± 0.016 (1σ) for Pb-T8, and $f_{Pa/U}$ = 3.36 ± 0.20 (1σ) for all samples. Given that the Quaternary zircons are essentially concordant, modified ^{207}Pb method (*82*) is conducted for correction of common Pb component. As isotopic composition of commmon Pb, $^{207}Pb/^{206}Pb$ = 0.8357 is used. In the case of secondary standards, $f_{Th/U}$ = 0.16 (typical value for zircon [*67*]) and $f_{Pa/U}$ = 3.36 ± 0.20 (1σ) are used for correction of initial disequilibrium, and isotopic compositions of common Pb of OD3 and Plešovice at their reported age are estimated by a two-stage model (*85*), as well.

Table S5. U-Pb isotopic and calculated age data on zircon grains (continued).

Sample name	Isotopic ratio				^{238}U-^{206}Pb age without correction (Ma)	1σ	Disequilibrium-corrected ^{238}U-^{206}Pb age (Ma)	1σ	Disequilibrium & common Pb-corrected U-Pb age (Ma)*	1σ	Elemental concentration (μg/g) and ratio					
	$^{206}Pb/^{238}U$	1σ	$^{207}Pb/^{206}Pb$	1σ							U	1σ	Th	1σ	Th/U	1σ
Zircons separated from BP-GB-BC-P1																
BP-GB-BC-P1 no.013	0.000143	0.000005	0.102	0.012	0.920	0.0	1.0	0.0	0.955	0.031	43.4	1.4	19.0	1.2	0.437	0.002
BP-GB-BC-P1 no.015	0.000150	0.000005	0.086	0.011	0.970	0.0	1.1	0.0	1.021	0.033	39.8	1.3	19.1	1.2	0.481	0.003
BP-GB-BC-P1 no.020	0.000148	0.000005	0.072	0.010	0.955	0.0	1.0	0.0	1.024	0.032	42.3	1.4	17.0	1.1	0.402	0.002
BP-GB-BC-P1 no.024	0.000142	0.000004	0.043	0.006	0.915	0.0	1.0	0.0	1.003	0.026	64.7	2.1	26.6	1.7	0.411	0.002
BP-GB-BC-P1 no.026	0.000137	0.000004	0.060	0.009	0.885	0.0	1.0	0.0	0.970	0.029	48.1	1.6	20.8	1.4	0.433	0.002
BP-GB-BC-P1 no.027	0.000137	0.000004	0.050	0.006	0.885	0.0	1.0	0.0	0.973	0.023	78.7	2.6	79.2	5.1	1.006	0.005
BP-GB-BC-P1 no.030	0.000154	0.000005	0.019	0.004	0.995	0.0	1.1	0.0	1.083	0.031	46.1	1.3	20.3	1.1	0.440	0.004
BP-GB-BC-P1 no.031	0.000166	0.000005	0.260	0.019	1.073	0.0	1.2	0.0	0.882	0.035	41.0	1.1	18.9	1.0	0.462	0.005
BP-GB-BC-P1 no.034	0.000146	0.000003	0.103	0.008	0.940	0.0	1.0	0.0	0.972	0.022	88.9	2.5	50.7	2.8	0.570	0.006
BP-GB-BC-P1 no.039	0.000145	0.000004	0.039	0.005	0.936	0.0	1.0	0.0	1.024	0.023	83.1	2.3	46.7	2.6	0.563	0.006
BP-GB-BC-P1 no.040	0.000135	0.000004	0.039	0.006	0.872	0.0	1.0	0.0	0.960	0.025	59.1	1.6	36.9	2.0	0.625	0.006
BP-GB-BC-P1 no.042	0.000137	0.000003	0.076	0.006	0.885	0.0	1.0	0.0	0.952	0.017	136.2	6.7	105.7	10.4	0.776	0.014
BP-GB-BC-P1 no.043	0.000122	0.000003	0.082	0.009	0.783	0.0	0.9	0.0	0.848	0.022	68.5	3.4	32.9	3.2	0.480	0.008
BP-GB-BC-P1 no.044	0.000154	0.000005	0.100	0.012	0.990	0.0	1.1	0.0	1.023	0.033	37.8	1.9	16.7	1.6	0.441	0.008
BP-GB-BC-P1 no.048	0.000143	0.000003	0.057	0.005	0.921	0.0	1.0	0.0	1.009	0.018	115.9	5.7	72.6	7.2	0.627	0.011
BP-GB-BC-P1 no.049	0.000138	0.000003	0.051	0.006	0.890	0.0	1.0	0.0	0.978	0.021	85.2	4.2	47.1	4.6	0.553	0.010
BP-GB-BC-P1 no.050	0.000150	0.000004	0.099	0.009	0.967	0.0	1.1	0.0	1.003	0.024	69.2	3.4	51.2	5.1	0.740	0.013
BP-GB-BC-P1 no.051	0.000142	0.000003	0.034	0.004	0.915	0.0	1.0	0.0	1.004	0.019	109.0	5.4	78.2	7.7	0.717	0.013
BP-GB-BC-P1 no.053	0.000132	0.000005	0.068	0.011	0.853	0.0	0.9	0.0	0.929	0.031	35.6	1.8	16.5	1.6	0.462	0.008
BP-GB-BC-P1 no.054	0.000132	0.000003	0.100	0.009	0.850	0.0	0.9	0.0	0.892	0.021	85.0	4.2	51.5	5.1	0.607	0.011
BP-GB-BC-P1 no.056	0.000129	0.000004	0.056	0.009	0.833	0.0	0.9	0.0	0.921	0.027	53.1	2.6	22.8	2.3	0.429	0.008
BP-GB-BC-P1 no.058	0.000157	0.000003	0.112	0.009	1.011	0.0	1.1	0.0	1.027	0.023	110.4	5.5	69.8	6.9	0.632	0.011
BP-GB-BC-P1 no.060	0.000154	0.000003	0.078	0.007	0.993	0.0	1.1	0.0	1.053	0.023	84.3	2.8	60.8	4.0	0.721	0.015
BP-GB-BC-P1 no.061	0.000174	0.000004	0.202	0.013	1.122	0.0	1.2	0.0	1.001	0.028	63.6	2.1	30.9	2.0	0.486	0.010
BP-GB-BC-P1 no.062	0.000143	0.000004	0.082	0.009	0.920	0.0	1.0	0.0	0.979	0.025	65.8	2.2	38.9	2.6	0.591	0.013
BP-GB-BC-P1 no.064	0.000171	0.000006	0.149	0.016	1.103	0.0	1.2	0.0	1.059	0.039	31.9	1.1	12.0	0.8	0.375	0.008
BP-GB-BC-P1 no.065	0.000150	0.000004	0.075	0.009	0.964	0.0	1.1	0.0	1.030	0.027	56.4	1.9	37.7	2.5	0.668	0.014
BP-GB-BC-P1 no.068	0.000141	0.000003	0.089	0.008	0.912	0.0	1.0	0.0	0.963	0.022	125.5	4.1	82.7	5.5	0.659	0.014
BP-GB-BC-P1 no.070	0.000161	0.000003	0.133	0.006	1.036	0.0	1.1	0.0	1.022	0.017	226.2	7.5	114.0	7.5	0.504	0.011
BP-GB-BC-P1 no.071	0.000146	0.000004	0.081	0.010	0.939	0.0	1.0	0.0	0.998	0.029	47.9	1.6	19.4	1.3	0.405	0.009
BP-GB-BC-P1 no.074	0.000151	0.000005	0.108	0.013	0.973	0.0	1.1	0.0	0.997	0.034	36.4	1.2	16.1	1.1	0.443	0.008
BP-GB-BC-P1 no.076	0.000130	0.000004	0.161	0.016	0.840	0.0	0.9	0.0	0.818	0.030	41.8	1.4	15.6	1.0	0.373	0.007
BP-GB-BC-P1 no.081	0.000158	0.000005	0.152	0.016	1.021	0.0	1.1	0.0	0.984	0.035	51.3	1.7	36.2	2.4	0.707	0.012
BP-GB-BC-P1 no.082	0.000176	0.000005	0.133	0.013	1.132	0.0	1.2	0.0	1.107	0.035	60.1	2.0	32.0	2.1	0.532	0.009
BP-GB-BC-P1 no.085	0.000162	0.000007	0.074	0.013	1.046	0.0	1.1	0.0	1.109	0.044	29.9	1.0	12.0	0.8	0.401	0.007
BP-GB-BC-P1 no.093	0.000144	0.000005	0.040	0.008	0.930	0.0	1.0	0.0	1.019	0.032	66.0	2.7	38.8	3.2	0.588	0.010
BP-GB-BC-P1 no.094	0.000138	0.000003	0.118	0.009	0.888	0.0	1.0	0.0	0.908	0.022	82.5	3.4	44.5	3.7	0.540	0.009
BP-GB-BC-P1 no.095	0.000136	0.000004	0.063	0.009	0.880	0.0	1.0	0.0	0.961	0.029	52.4	2.2	23.2	1.9	0.442	0.008
BP-GB-BC-P1 no.097	0.000152	0.000003	0.159	0.008	0.978	0.0	1.1	0.0	0.939	0.018	134.8	5.5	53.7	4.4	0.398	0.007
BP-GB-BC-P1 no.101	0.000160	0.000004	0.143	0.011	1.030	0.0	1.1	0.0	1.004	0.025	74.8	3.1	30.3	2.5	0.405	0.007
BP-GB-BC-P1 no.102	0.000137	0.000004	0.117	0.011	0.884	0.0	1.0	0.0	0.904	0.025	66.0	2.7	38.6	3.2	0.584	0.010
BP-GB-BC-P1 no.109	0.000142	0.000004	0.049	0.008	0.918	0.0	1.0	0.0	1.006	0.028	64.5	3.4	33.4	3.5	0.517	0.011
BP-GB-BC-P1 no.111	0.000178	0.000005	0.262	0.017	1.150	0.0	1.2	0.0	0.936	0.033	50.4	2.7	23.7	2.5	0.470	0.010
BP-GB-BC-P1 no.112	0.000144	0.000003	0.081	0.006	0.927	0.0	1.0	0.0	0.987	0.019	151.6	8.0	102.5	10.8	0.676	0.015
BP-GB-BC-P1 no.116	0.000139	0.000004	0.146	0.011	0.897	0.0	1.0	0.0	0.884	0.024	69.6	3.7	42.9	4.5	0.616	0.013
BP-GB-BC-P1 no.119	0.000136	0.000003	0.096	0.009	0.874	0.0	1.0	0.0	0.919	0.022	78.1	4.1	38.5	4.1	0.493	0.011
BP-GB-BC-P1 no.120	0.000157	0.000005	0.303	0.020	1.011	0.0	1.1	0.0	0.782	0.032	48.6	2.6	22.2	2.4	0.457	0.010
			Wtd. mean ± 1σ		**0.937 ± 0.011**		**1.026 ± 0.011**		**0.971 ± 0.009**							
			MSWD		**9.4**		**7.4**		**5.9**							
			n		**47**		**47**		**47**							
Zircons separated from Pb-T8																
Pb-T8 no.001	0.000278	0.000005	0.036	0.003	1.789	0.032	1.860	0.032	1.860	0.032	49.1	2.8	24.9	2.9	0.508	0.012
Pb-T8 no.004	0.000346	0.000004	0.228	0.006	2.227	0.024	2.298	0.024	1.796	0.025	110.1	6.4	77.3	9.0	0.703	0.017
Pb-T8 no.006	0.000271	0.000003	0.097	0.003	1.745	0.018	1.816	0.018	1.713	0.018	156.0	9.0	134.9	15.6	0.864	0.021
Pb-T8 no.009	0.000251	0.000003	0.064	0.002	1.615	0.017	1.686	0.017	1.659	0.017	170.6	9.9	123.1	14.3	0.721	0.018
Pb-T8 no.015	0.000247	0.000002	0.051	0.001	1.595	0.010	1.666	0.011	1.666	0.011	575.5	33.4	884.4	102.5	1.537	0.038
Pb-T8 no.018	0.000303	0.000005	0.247	0.008	1.953	0.029	2.024	0.029	1.537	0.029	62.7	3.6	33.2	3.8	0.530	0.013
Pb-T8 no.022	0.000252	0.000003	0.093	0.003	1.626	0.018	1.697	0.018	1.612	0.018	146.9	8.5	97.1	11.3	0.661	0.016
Pb-T8 no.023	0.000951	0.000006	0.636	0.014	6.130	0.041	6.201	0.041	1.633	0.106	149.4	8.7	73.5	8.5	0.492	0.012
Pb-T8 no.024	0.000246	0.000003	0.064	0.003	1.585	0.020	1.656	0.021	1.631	0.020	103.9	6.0	54.5	6.3	0.525	0.013
Pb-T8 no.027	0.000265	0.000003	0.076	0.002	1.708	0.016	1.778	0.016	1.725	0.016	188.4	10.9	158.4	18.4	0.841	0.021
Pb-T8 no.030	0.000295	0.000003	0.173	0.004	1.902	0.017	1.973	0.017	1.677	0.017	212.3	12.3	212.0	24.6	0.998	0.024
Pb-T8 no.033	0.000301	0.000003	0.192	0.005	1.941	0.018	2.012	0.018	1.664	0.019	178.5	10.3	139.0	16.1	0.778	0.019
Pb-T8 no.035	0.000274	0.000004	0.092	0.003	1.768	0.024	1.838	0.024	1.746	0.023	159.5	3.6	124.1	5.5	0.778	0.018
Pb-T8 no.036	0.000251	0.000004	0.059	0.002	1.620	0.023	1.691	0.023	1.674	0.023	132.8	3.0	91.3	4.1	0.687	0.016
Pb-T8 no.037	0.000301	0.000004	0.178	0.005	1.941	0.026	2.012	0.026	1.698	0.024	150.8	3.4	104.0	4.6	0.689	0.016
Pb-T8 no.039	0.000257	0.000003	0.060	0.001	1.659	0.017	1.730	0.017	1.711	0.016	2909.3	65.0	7556.7	337.5	2.597	0.061
Pb-T8 no.040	0.000318	0.000004	0.237	0.006	2.049	0.026	2.119	0.026	1.636	0.024	183.2	4.1	140.5	6.3	0.767	0.018
Pb-T8 no.049	0.000260	0.000003	0.104	0.003	1.675	0.022	1.746	0.022	1.634	0.021	177.5	4.0	131.0	5.9	0.738	0.017
Pb-T8 no.050	0.000253	0.000003	0.109	0.003	1.632	0.021	1.703	0.021	1.584	0.020	198.7	4.4	147.9	6.6	0.744	0.018
Pb-T8 no.053	0.000280	0.000003	0.137	0.003	1.806	0.020	1.877	0.020	1.679	0.019	542.9	12.1	483.8	21.6	0.891	0.021
Pb-T8 no.054	0.000252	0.000003	0.049	0.001	1.624	0.016	1.694	0.017	1.694	0.017	3344.9	74.7	6843.3	305.6	2.046	0.048
Pb-T8 no.062	0.000348	0.000006	0.240	0.008	2.244	0.041	2.314	0.041	1.773	0.037	47.4	1.1	14.7	0.7	0.309	0.007
Pb-T8 no.064	0.000284	0.000004	0.139	0.004	1.833	0.024	1.903	0.024	1.698	0.022	170.4	3.8	132.8	5.9	0.779	0.018
Pb-T8 no.065	0.000258	0.000004	0.094	0.003	1.660	0.024	1.731	0.024	1.642	0.023	136.7	3.1	94.1	4.2	0.688	0.016
Pb-T8 no.070	0.000262	0.000002	0.081	0.001	1.691	0.015	1.762	0.016	1.698	0.015	3724.9	83.6	4703.1	211.1	1.263	0.011
Pb-T8 no.072	0.000265	0.000004	0.061	0.002	1.711	0.023	1.782	0.023	1.761	0.022	141.0	3.2	111.2	5.0	0.789	0.007
Pb-T8 no.076	0.000273	0.000003	0.113	0.002	1.762	0.022	1.833	0.022	1.694	0.020	176.2	4.0	129.7	5.8	0.736	0.006
Pb-T8 no.078	0.000257	0.000002	0.059	0.001	1.656	0.015	1.727	0.015	1.711	0.015	3192.0	71.6	6916.6	310.5	2.167	0.019
Pb-T8 no.079	0.000291	0.000003	0.128	0.002	1.878	0.022	1.949	0.022	1.766	0.020	228.3	5.1	168.7	7.6	0.739	0.007
Pb-T8 no.084	0.000496	0.000005	0.408	0.005	3.194	0.035	3.265	0.036	1.811	0.028	168.1	3.8	232.1	10.4	1.381	0.012
Pb-T8 no.090	0.000365	0.000004	0.288	0.004	2.351	0.027	2.422	0.028	1.712	0.022	173.9	3.9	127.5	5.7	0.733	0.006
			Wtd. mean ± 1σ		**1.79 ± 0.08**		**1.86 ± 0.08**		**1.688 ± 0.010**							
			MSWD		**503**		**493**		**7.5**							
			n		**31**		**31**		**31**							

* Corrected ages are calculated considering both the effect of initial disequilibrium and the common Pb contribution (see text for explanation). As estimation of Th/U and Pa/U partioning in zircon-melt system, following values are applied: $f_{Th/U}$ = 0.194 ± 0.014 (1σ) for BP-LMTCL-1, $f_{Th/U}$ = 0.185 ± 0.017 (1σ) for BP-GB-BC-P1, and $f_{Th/U}$ = 0.351 ± 0.016 (1σ) for Pb-T8, and $f_{Pa/U}$ = 3.36 ± 0.20 (1σ) for all samples. Given that the Quaternary zircons are essentially concordant, modified ^{207}Pb method (*82*) is conducted for correction of common Pb component. As isotopic composition of commmon Pb, $^{207}Pb/^{206}Pb$ = 0.8357 is used. In the case of secondary standards, $f_{Th/U}$ = 0.16 (typical value for zircon [*67*]) and $f_{Pa/U}$ = 3.36 ± 0.20 (1σ) are used for correction of initial disequilibrium, and isotopic compositions of common Pb of OD3 and Plešovice at their reported age are estimated by a two-stage model (*85*), as well.

Table S5. U-Pb isotopic and calculated age data on zircon grains (continued).

Sample name	Isotopic ratio				^{238}U-^{206}Pb age without correction (Ma)		Disequilibrium-corrected ^{238}U-^{206}Pb age (Ma)		Disequilibrium & common Pb-corrected U-Pb age (Ma)*		Elemental concentration (µg/g) and ratio					
	$^{206}Pb/^{238}U$	1σ	$^{207}Pb/^{206}Pb$	1σ		1σ		1σ		1σ	U	1σ	Th	1σ	Th/U	1σ
OD3 zircons as secondary reference material																
OD3-1	0.005289	0.000039	0.0469	0.0009	34.0	0.3	34.10	0.29	34.10	0.34	81.0	2.0	52.4	2.6	0.647	0.005
OD3-2	0.005076	0.000026	0.0459	0.0007	32.6	0.2	32.73	0.21	32.73	0.25	139.6	2.0	119.5	3.4	0.856	0.007
OD3-3	0.005094	0.000027	0.0473	0.0006	32.8	0.2	32.84	0.22	32.83	0.18	213.6	2.3	194.6	4.1	0.911	0.006
OD3-4	0.005167	0.000036	0.0462	0.0006	33.2	0.2	33.31	0.28	33.31	0.32	232.3	7.0	229.1	13.7	0.986	0.011
OD3-5	0.005074	0.000026	0.0465	0.0005	32.6	0.2	32.72	0.21	32.72	0.25	279.8	4.0	279.6	8.0	0.999	0.008
OD3-6	0.005026	0.000040	0.0467	0.0004	32.3	0.3	32.41	0.30	32.41	0.34	536.9	8.4	747.6	23.3	1.392	0.012
OD3-7	0.005074	0.000027	0.0470	0.0005	32.6	0.2	32.72	0.21	32.71	0.17	340.2	28.4	358.7	60.0	1.054	0.020
OD3-8	0.005039	0.000033	0.0471	0.0005	32.4	0.2	32.49	0.25	32.49	0.21	333.8	2.9	336.5	5.8	1.008	0.013
OD3-9	0.005042	0.000035	0.0468	0.0005	32.4	0.2	32.51	0.27	32.51	0.31	338.7	3.8	363.5	8.1	1.073	0.009
OD3-10	0.005114	0.000051	0.0469	0.0005	32.9	0.3	32.97	0.37	32.97	0.41	293.6	9.5	310.0	20.2	1.056	0.006
OD3-11	0.005100	0.000051	0.0477	0.0004	32.8	0.3	32.88	0.37	32.85	0.32	531.9	14.7	752.6	41.5	1.415	0.014
OD3-12	0.005122	0.000017	0.0493	0.0004	32.9	0.1	33.02	0.15	32.92	0.11	544.4	26.9	777.2	76.7	1.428	0.025
OD3-13	0.005123	0.000028	0.0468	0.0005	32.9	0.2	33.03	0.22	33.03	0.27	307.5	10.1	336.2	22.2	1.093	0.023
OD3-14	0.005054	0.000035	0.0466	0.0007	32.5	0.2	32.59	0.27	32.59	0.31	174.7	5.7	137.7	9.0	0.788	0.014
OD3-15	0.005155	0.000028	0.0520	0.0007	33.1	0.2	33.23	0.22	33.02	0.18	150.5	6.2	110.2	9.1	0.732	0.013
OD3-16	0.005105	0.000029	0.0464	0.0004	32.8	0.2	32.91	0.23	32.91	0.27	547.3	29.0	637.8	67.5	1.165	0.025
OD3-17	0.005097	0.000065	0.0457	0.0002	32.8	0.4	32.87	0.42	32.87	0.42	513.0	9.8	575.6	22.0	1.122	0.012
OD3-18	0.005221	0.000067	0.0452	0.0003	33.6	0.4	33.66	0.43	33.66	0.43	254.3	4.9	246.5	9.4	0.969	0.011
OD3-19	0.005090	0.000066	0.0463	0.0003	32.7	0.4	32.82	0.42	32.82	0.42	235.7	4.5	225.7	8.6	0.958	0.011
OD3-20	0.005172	0.000047	0.0467	0.0004	33.3	0.3	33.35	0.30	33.35	0.30	244.6	5.5	237.2	10.6	0.970	0.009
OD3-21	0.005093	0.000046	0.0466	0.0004	32.8	0.3	32.84	0.29	32.84	0.29	488.8	11.0	553.6	24.9	1.133	0.010
OD3-22	0.005115	0.000046	0.0459	0.0004	32.9	0.3	32.98	0.30	32.98	0.30	482.4	10.8	528.9	23.7	1.097	0.010
OD3-23	0.005069	0.000045	0.0459	0.0004	32.6	0.3	32.69	0.29	32.69	0.29	556.3	12.5	609.6	27.4	1.096	0.010
			Wtd. mean ± 1σ		**32.82 ± 0.07**		**32.92 ± 0.08**		**32.88 ± 0.07**							
				MSWD	**2.4**		**1.8**		**1.4**							
				n	**23**		**23**		**23**							
Plešovice zircons as secondary reference material																
Plešovice-1	0.05353	0.00034	0.05317	0.00026	336.2	2.1	336.2	2.6	336.2	3.0	826	21	110	6	0.1327	0.0010
Plešovice-2	0.05330	0.00023	0.05318	0.00028	334.7	1.4	334.8	1.8	334.8	2.3	804	11	100	3	0.1246	0.0010
Plešovice-3	0.05312	0.00026	0.05312	0.00027	333.7	1.6	333.8	2.0	333.8	2.5	832	9	104	2	0.1252	0.0008
Plešovice-4	0.05286	0.00035	0.05315	0.00011	332.0	2.2	332.1	2.6	332.1	3.0	898	27	119	7	0.1328	0.0014
Plešovice-5	0.05302	0.00025	0.05294	0.00011	333.0	1.6	333.1	2.0	333.1	2.4	894	13	120	3	0.1341	0.0011
Plešovice-6	0.05313	0.00041	0.05334	0.00014	333.7	2.5	333.8	3.0	333.8	3.4	876	14	113	4	0.1291	0.0011
Plešovice-7	0.05307	0.00026	0.05310	0.00021	333.3	1.6	333.4	2.0	333.4	2.5	1077	90	132	22	0.1224	0.0024
Plešovice-8	0.05386	0.00034	0.05325	0.00015	338.2	2.1	338.3	2.5	338.3	2.9	970	8	126	2	0.1304	0.0017
Plešovice-9	0.05339	0.00036	0.05344	0.00015	335.3	2.2	335.4	2.6	335.4	3.1	954	11	126	3	0.1319	0.0011
Plešovice-10	0.05345	0.00052	0.05348	0.00024	335.7	3.2	335.8	3.6	335.8	4.0	996	32	127	8	0.1276	0.0007
Plešovice-11	0.05362	0.00053	0.05307	0.00014	336.7	3.2	336.8	3.7	336.8	4.1	975	27	126	7	0.1292	0.0013
Plešovice-12	0.05307	0.00016	0.05324	0.00016	333.3	1.0	333.4	1.4	333.4	1.8	983	49	127	13	0.1290	0.0023
Plešovice-13	0.05348	0.00028	0.05356	0.00014	335.9	1.7	336.0	2.1	336.0	2.6	940	31	120	8	0.1278	0.0027
Plešovice-14	0.05367	0.00035	0.05331	0.00017	337.0	2.1	337.1	2.6	337.1	3.0	980	32	127	8	0.1298	0.0023
Plešovice-15	0.05363	0.00025	0.05339	0.00016	336.8	1.5	336.9	2.0	336.9	2.4	1008	41	130	11	0.1292	0.0022
Plešovice-16	0.05317	0.00029	0.05327	0.00017	333.9	1.8	334.0	2.2	334.0	2.7	1049	55	133	14	0.1268	0.0027
Plešovice-17	0.05460	0.00070	0.05289	0.00016	342.7	4.3	342.8	4.3	342.8	4.3	433	8	38	1	0.0885	0.0010
Plešovice-18	0.05412	0.00069	0.05389	0.00017	339.8	4.2	339.9	4.2	339.9	4.2	435	8	41	2	0.0941	0.0010
Plešovice-19	0.05431	0.00069	0.05270	0.00016	340.9	4.2	341.0	4.2	341.0	4.2	418	8	38	1	0.0897	0.0010
Plešovice-20	0.05353	0.00048	0.05269	0.00041	336.2	2.9	336.2	2.9	336.2	2.9	409	9	36	2	0.0881	0.0008
Plešovice-21	0.05372	0.00048	0.05240	0.00041	337.3	2.9	337.4	2.9	337.4	2.9	423	9	37	2	0.0879	0.0008
Plešovice-22	0.05389	0.00048	0.05303	0.00042	338.4	2.9	338.5	3.0	338.5	3.0	432	10	39	2	0.0895	0.0008
Plešovice-23	0.05387	0.00048	0.05377	0.00042	338.2	2.9	338.3	3.0	338.3	3.0	428	10	38	2	0.0897	0.0008
			Wtd. mean ± 1σ		**335.0 ± 0.4**		**335.4 ± 0.5**		**335.6 ± 0.6**							
				MSWD	**1.1**		**0.84**		**0.69**							
				n	**23**		**23**		**23**							

* Corrected ages are calculated considering both the effect of initial disequilibrium and the common Pb contribution (see text for explanation). As estimation of Th/U and Pa/U partioning in zircon-melt system, following values are applied: $f_{Th/U}$ = 0.194 ± 0.014 (1σ) for BP-LMTCL-1, $f_{Th/U}$ = 0.185 ± 0.017 (1σ) for BP-GB-BC-P1, and $f_{Th/U}$ = 0.351 ± 0.016 (1σ) for Pb-T8, and $f_{Pa/U}$ = 3.36 ± 0.20 (1σ) for all samples. Given that the Quaternary zircons are essentially concordant, modified ^{207}Pb method (*82*) is conducted for correction of common Pb component. As isotopic composition of commmon Pb, $^{207}Pb/^{206}Pb$ = 0.8357 is used. In the case of secondary standards, $f_{Th/U}$ = 0.16 (typical value for zircon [*67*]) and $f_{Pa/U}$ = 3.36 ± 0.20 (1σ) are used for correction of initial disequilibrium, and isotopic compositions of common Pb of OD3 and Plešovice at their reported age are estimated by a two-stage model (*85*), as well.